Received: 28 January 2020 | Revised: 30 April 2020 | Accepted: 30 April 2020

DOI: 10.1002/cne.24941

RESEARCH ARTICLE

JCN RESEARCH IN SYSTEMS NEUROSCIENCE THE JOURNAL OF COMPARATIVE NEUROLOGY WILEY

Neuroarchitecture of the central complex in the brain of the honeybee: Neuronal cell types

Ronja Hensgen[1] | Laura England[1] | Uwe Homberg[1] | Keram Pfeiffer[2]

[1]Animal Physiology, Department of Biology, Philipps-Universität Marburg, Marburg, Germany

[2]Behavioral Physiology and Sociobiology (Zoology II), Biozentrum, University of Würzburg, Würzburg, Germany

Correspondence
Keram Pfeiffer, Behavioral Physiology and Sociobiology (Zoology II), Biozentrum, University of Würzburg, Am Hubland, Würzburg 97074, Germany.
Email: keram.pfeiffer@uni-wuerzburg.de

Funding information
Deutsche Forschungsgemeinschaft, Grant/Award Numbers: HO950/24-1, PF714/4-1

Peer Review
The peer review history for this article is available at https://publons.com/publon/10.1002/cne.24941.

Abstract

The central complex (CX) in the insect brain is a higher order integration center that controls a number of behaviors, most prominently goal directed locomotion. The CX comprises the protocerebral bridge (PB), the upper division of the central body (CBU), the lower division of the central body (CBL), and the paired noduli (NO). Although spatial orientation has been extensively studied in honeybees at the behavioral level, most electrophysiological and anatomical analyses have been carried out in other insect species, leaving the morphology and physiology of neurons that constitute the CX in the honeybee mostly enigmatic. The goal of this study was to morphologically identify neuronal cell types of the CX in the honeybee *Apis mellifera*. By performing iontophoretic dye injections into the CX, we traced 16 subtypes of neuron that connect a subdivision of the CX with other regions in the bee's central brain, and eight subtypes that mainly interconnect different subdivisions of the CX. They establish extensive connections between the CX and the lateral complex, the superior protocerebrum and the posterior protocerebrum. Characterized neuron classes and subtypes are morphologically similar to those described in other insects, suggesting considerable conservation in the neural network relevant for orientation.

KEYWORDS

Apis mellifera, RRID: AB_2337244, RRID: AB_2315425, central complex, insect brain, neuroanatomy, sky compass

1 | INTRODUCTION

Spatial orientation and its underlying neural mechanisms have been intensely studied in different insect species. During goal-directed behaviors animals are constantly challenged to keep track of their orientation and body position with respect to an external reference frame. Different orientation strategies have been analyzed at the behavioral level, for example, for straight-line orientation in ball-rolling dung beetles (for review see el Jundi, Baird, Byrne, & Dacke, 2019), path-integration in desert ants (for review see Heinze, Narendra, & Cheung, 2018) and sky compass orientation in honeybees (von Frisch, 1949).

ABBREVIATIONS: AL, antennal lobe; ALl, anterior lip; CB, central body; CBL, lower division of the central body; CBU, upper division of the central body; CRE, crepine; CX, central complex; LAL, lateral accessory lobe; LBU, lateral bulb; LCA, lateral calyx of the mushroom body; LX, lateral complex; MB, mushroom body; MBU, medial bulb; MCA, medial calyx of the mushroom body; ML, medial lobe of the mushroom body; NO, noduli; NOL, lower unit of the nodulus; NOU, upper unit of the nodulus; PB, protocerebral bridge; PI, pars intercerebralis; PS, posterior slope; SIP, superior intermediate protocerebrum; SLP, superior lateral protocerebrum; SMP, superior medial protocerebrum; VL, vertical lobe of the mushroom body.

A multitude of sensory cues likely serves to navigate to a distant target and has to be processed and integrated appropriately. In insects, the central complex (CX) in the center of the protocerebrum is thought to provide many of the required computational functions illustrated by its key role in spatial orientation memory (Neuser, Triphan, Mronz, Poeck, & Strauss, 2008), place memory (Ofstad, Zuker, & Reiser, 2011), angular integration (Green et al., 2017; Turner-Evans et al., 2017), and sky compass orientation (el Jundi, Pfeiffer, Heinze, & Homberg, 2014; Heinze & Homberg, 2007; Pegel, Pfeiffer, & Homberg, 2018). Its influence on locomotor activity, especially decisions on heading direction, has been demonstrated in cockroaches (Bender, Pollack, & Ritzmann, 2010; Guo & Ritzmann, 2013) and flies (Buchanan, Kain, & de Bivort, 2015; Green, Vijayan, Mussells Pires, Adachi, & Maimon, 2019; Poeck, Triphan, Neuser, & Strauss, 2008; Strauss & Heisenberg, 1993), and a variety of additional functions were demonstrated that point to the CX as a higher integration center (for review see Pfeiffer & Homberg, 2014).

Anatomically, the CX is an assembly of neuropils spanning the brain midline. It is composed of the protocerebral bridge (PB), the upper division (CBU), and the lower division (CBL) of the central body and a bilateral pair of noduli (NO; Pfeiffer & Homberg, 2014). Projection patterns of neurons constituting the CX result in its characteristic organization defined by horizontal layers (for CBU, CBL, and NO) and 16–18 vertical slices (for PB, CBU, and CBL; Heinze & Homberg, 2008; Wolff, Iyer, & Rubin, 2015). Tangential neurons with arborizations in different brain regions innervate entire horizontal layers, likely providing input to the CX network (Hanesch, Fischbach, & Heisenberg, 1989; Honkanen, Adden, da Silva Freitas, & Heinze, 2019; von Hadeln et al., 2020). Columnar neurons innervate the vertical slices of the CX neuropils, and many types have additional ramifications in the noduli or lateral complex (Hanesch et al., 1989; Heinze & Homberg, 2008; Wolff, Iyer, & Rubin, 2015). For most types of columnar neuron, a set of 16–18 individual cells follows a stereotypical, interhemispheric wiring scheme (Heinze & Homberg, 2008; Honkanen et al., 2019; Wolff, Iyer, & Rubin, 2015). The neuroarchitecture of the CX is highly conserved in most insect species examined to date (el Jundi, Warrant, Pfeiffer, & Dacke, 2018; Heinze, Florman, Asokaraj, el Jundi, & Reppert, 2013; Heinze & Homberg, 2008; Wolff & Rubin, 2018).

Although honeybees show sophisticated orientation abilities, impressively illustrated by their capability to communicate direction and distance of a food source to their hive mates (Barron & Plath, 2017; von Frisch, 1946), surprisingly little is known about the physiology and anatomy of the honeybee's CX. Information about its organization largely originates from early anatomical studies (Jonescu, 1909; Mobbs, 1985), two electrophysiological investigations (Homberg, 1985; Milde, 1988), and various reports on the distribution of neuroactive substances (Schäfer & Bicker, 1986; Schürmann & Klemm, 1984; Sinakevitch, Niwa, & Strausfeld, 2005; Kreissl, Strasser, & Galizia, 2010). Intracellular recordings showed that various CX neurons of the honeybee respond weakly to simple visual stimuli, some neurons also to mechanical stimulation of antennae or abdomen. More recently, tracing studies demonstrated that, like in other insects, the honeybee CX is specifically targeted by neural pathways originating in the dorsal rim of the medulla, likely serving a role in sky compass navigation (Held et al., 2016; Zeller et al., 2015). The final stage of this pathway are neurons that connect two small areas in the lateral complex (LX), the medial and lateral bulbs, to the CBL (Held et al., 2016). A proposed role of the honeybee CX in spatial orientation is further supported by an electrophysiological and computational study in the related sweat bee *Megalopta genalis*, providing evidence for a role of the CX in path integration (Stone et al., 2017). To complement previous work on the neuroanatomy of the sky compass pathway and to provide a more detailed anatomical basis for further functional studies, we analyzed the morphology of neuronal cell types in the honeybee CX. While some of the cell types are similar to those found in other species, a few types of neuron are described here for the first time.

2 | MATERIALS AND METHODS

2.1 | Animals

Forager honeybees were collected at the entrance of the hive, maintained at the Department of Biology at the Philipps-University Marburg. Between October and March, the bee hive was kept inside a greenhouse under natural light/dark conditions at 25 °C. Bees could fly freely within a space of 2 m × 2 m × 2 m and were supplied with honey water (20–30%) and pollen. From March to October, the bee hive was kept outside.

2.2 | Preparation

Bees were cold anesthetized in a refrigerator. They were attached to a holder with dental wax. To expose the brain, the head capsule was opened frontally between the compound eyes. Tracheae, air sacs and glands were removed. To prevent movement of the brain, muscles within the head capsule were transected and the gut was removed. The neural sheath was removed above the central brain to allow brain tissue penetration by the injection electrode. During preparation, the brain was constantly covered with honeybee saline (containing in mM: NaCl 130, KCl 5, $MgCl_2$ 4, HEPES 15, glucose 25, sucrose 160, adjusted to pH 7.2).

2.3 | Immunolabeling of whole-mounts

To label synapse-dense areas in whole-mount brains we used a protocol modified after Ott (2008). As for dye-injections the head capsule was opened and tissue around the brain was removed. Instead of honeybee saline, HEPES-buffered saline (HBS; 150 mM NaCl, 5 mM KCl, 5 mM $CaCl_2$, 25 mM sucrose, 10 mM HEPES (4-[2-hydroxyethyl]-1-piperazineethanesulfonic acid)) (Heidel & Pflüger, 2006) was used to perfuse the brain. The brains were exposed to zinc-formaldehyde

(ZnFA; 18.4 mM $ZnCl_2$, 135 mM NaCl, 35 mM sucrose, and 1% formaldehyde; Ott, 2008) for 1 hr, then the head was cut off and fixed for 20 hr at room temperature. Brains were dissected from the head capsule under HBS and rinsed in HBS (8 × 25 min). Afterward they were rinsed in TRIS buffer (pH 7.4) (3 × 10 min), incubated for 85–90 min in 20% dimethyl sulfoxide (DMSO)/80% methanol (Dent's fixative; Dent, Polson, & Klymkowsky, 1989), and rinsed again in TRIS buffer (3 × 10 min). To block non-specific binding of antibodies, brains were incubated overnight in 5% normal goat serum (NGS) in PBSTD (0.01 M phosphate-buffered saline (PBS, pH 7.4) with 1% DMSO and 0.3% Triton X-100 (TrX; Sigma, Deisenhofen, Germany) at 4 °C. Brains were incubated for 7–8 days at 4 °C with a monoclonal antibody against synapsin I (1: 50, SYNORF1, kindly provided by Drs. E. Buchner and C. Wegener, University of Würzburg, Germany, RRID: AB_2315425), 1% NGS and 0.02% NaN_3 in 0.01 M PBSTD.

The monoclonal antibody against synapsin was raised in mice against fusion proteins consisting of glutathione-*S*-transferase and parts of the *Drosophila* synaptic vesicle protein SYN1 (Klagges et al., 1996). The antibody has been used to label synaptic neuropils in different insect species, including honeybees (Brandt et al., 2005). The specificity of the antibody has been shown in *Drosophila* by Klagges et al. (1996).

Following incubation brains were rinsed in PBSTD (8 × 30 min) and incubated with goat-anti-mouse antiserum conjugated to Cy5 (1:300, Dianova, Hamburg, Germany), 1% NGS and 0.02% NaN_3 in 0.01 M PBSTD for 8 days at 4 °C. After rinsing in PBSTD (6 × 30 min) and PBS (2 × 30 min) brains were dehydrated in an ascending ethanol series (30, 50, 70, 90, 95, 100%, 15 min each). To clear the brains, they were transferred to a 1:1 mixture of 100% ethanol and methyl salicylate for 15–20 min followed by pure methyl salicylate for 60 min. Finally, the brains were mounted between two coverslips using Permount (Fisher Scientific, Pittsburgh, PA). To prevent compression of the brain, eight reinforcement rings (Zweckform, Oberlaindern, Germany) were stacked to serve as spacers.

2.4 | Extracellular iontophoretic dye injection

To stain small numbers of neurons (1–20) with processes in the CX, extracellular iontophoretic dye injections were performed as described in Held et al. (2016). Sharp micropipettes with resistances between 80 and 300 MΩ were drawn from borosilicate glass (inner diameter 0.75 mm, outer diameter 1.5 mm, Hilgenberg, Malsfeld, Germany) using a Flaming/Brown horizontal puller (P-97, Sutter Instrument, Novato, CA). Electrode tips were filled with 4% Neurobiotin (Vector Laboratories, Burlingame, CA) in 1 M KCl and backed up with 2.5 M KCl. A chlorinated silver wire was submerged in the saline solution to act as a reference electrode. Injection electrodes were inserted frontally into the brain and positioned in the area of the CX using a micromanipulator (Leica Microsystems, Wetzlar, Germany). The tracer was ejected from the electrode by applying rectangular positive current pulses of 10 nA (1 Hz, 50% duty cycle) for 20–45 min. The electroporating effect of the electric field presumably allowed the tracer to enter neurons in the vicinity of the tip. After removing the electrode honeybee saline was substituted by a fixative solution of 4% paraformaldehyde (Sigma-Aldrich, Steinheim, Germany), 0.25% glutaraldehyde (Carl Roth, Karlsruhe, Germany), and 0.25% saturated picric acid in 0.1 M PBS. The brains were dissected from the head capsule and submerged in fixative overnight at 4°C. After washing in PBS (4 × 15 min) brains were incubated with Cy3-conjugated streptavidin (1:1,000, Jackson ImmunoResearch, RRID: AB_2337244) in 0.1 M PBT (0.1 M PBS with 0.3% TrX) for 3 days at 4 °C. Brains were then washed with PBT (2 × 30 min) and PBS (3 × 30 min). Dehydration and mounting were performed as described for immunolabeling of whole-mounts.

2.5 | Immunolabeling on sections from rehydrated brains

To study successfully stained neurons in more detail, we selected some of the brains for further processing. Embedded brains were incubated in xylene for 1–3 hr at room temperature to remove Permount, dehydrated using a descending ethanol series (100, 95, 90, 70, 50, and 30%), washed in 0.1 M PBS (3 × 15 min) and embedded in albumin/gelatin (12% ovalbumin, 4.8% gelatin in demineralized water). After fixation overnight at 4 °C with 8% formaldehyde in 0.1 M sodium phosphate buffer (NaPi; pH 7.4) brains were sectioned at 130 μm in the frontal plane using a vibrating blade microtome (VT1200 S, Leica Microsystems, Wetzlar, Germany). Sections were washed in 0.01 M PBS (2 × 10 min), 0.01 M PBT (4 × 10 min) and preincubated with 5% NGS, in 0.01 M PBT overnight at 4°C. The primary antibody solution was applied for 5 days at 4°C. It contained the SYNORF1 antibody (1:50) in 0.01 M PBT.

Following rinsing with 0.01 M PBT (6 × 10 min) sections were incubated overnight at 4°C with a solution consisting of goat-anti-mouse antiserum conjugated to Cy5 (1:300), streptavidin conjugated to Cy3 (1:1,000) and 1% NGS in 0.01 M PBT. After washing with 0.01 M PBT (4 × 15 min), 0.01 M PBS (2 × 15 min), and dehydrating in an ascending ethanol series (30, 50, 70, 90, 95, and 100%, 5 min each) sections were cleared in ethanol and methyl salicylate (1:1, 5 min) and pure methyl salicylate (15 min). Using stacks of two reinforcement rings, sections were embedded in Permount between two coverslips.

2.6 | Image acquisition

Image stacks were obtained with a confocal laser scanning microscope (CLSM; TCS SP5, Leica Microsystems, Wetzlar, Germany). Whole mount preparations were scanned with a 10× or a 20× oil immersion objective (HC PL APO 10×/0.40 IMM CS, HCX PL APO 20×/0.70 Imm Corr Lbd. bl.) or a 63× glycerol immersion objective (HCX PL APO 63×/1.3 GLY CORR CS 21). A 40× oil immersion objective (HCX PL APO 40×/1.25–0.75 Oil Lbd. BI; all objectives: Leica) or the 63× glycerol immersion objective were used to acquire images of gelatin

sections. All samples were scanned at a resolution of 1,024 × 1,024 pixels per image, a scanning frequency of 200 Hz and a pinhole size of 1 Airy unit. The *z*-step size was set between 0.5 and 3 μm. Excitation of the fluorophores was achieved using a helium neon laser (633 nm, Cy5) or a diode-pumped solid-state (DPSS) laser (561 nm, Cy3).

2.7 | 3D reconstructions

Primary processing of all image stacks was done with the software Amira (5.6 and 6.0; FEI Visualization Sciences Group, Mérignac Cedex, France, now part of Thermo Fisher Scientific Inc.). 3D reconstruction of neuropils was based on anti-synapsin labeling. In the Segmentation Editor the neuropil of interest was marked manually in several optical slices in the *x*-, *y*-, and *z*-planes. The scaffold was extrapolated into a 3D structure using the wrapping function. In the Object Pool polygonal surfaces were generated with the module SurfaceGen and displayed via the module SurfaceView. 3D reconstruction of single neurons was based on Neurobiotin injections. All processes of a cell were manually traced using the skeletonize plugin for Amira (Evers, Schmitt, Sibila, & Duch, 2005; Schmitt, Evers, Duch, Scholz, & Obermayer, 2004). Diameter and midline of each neuronal segment were adjusted by applying an integrated fitting algorithm. To visualize the morphology of multiple neurons the neuronal staining was manually selected in each optical slice in the Segmentation Editor. The background was masked using the module Arithmetic in the Object Pool. Remaining areas were then visualized by intensity-based direct volume rendering using the module Voltex.

3 | RESULTS

3.1 | Nomenclature and general anatomy

Neuropils are named following the nomenclature for the fruit fly (Ito et al., 2014) that has also been adapted for other insects (e.g., locusts, von Hadeln, Althaus, Häger, & Homberg, 2018; dung beetles, Immonen, Dacke, Heinze, & el Jundi, 2017). Figure 1 depicts the organization of the honeybee CX and some of the associated neuropils. As in other species, the CX of the honeybee comprises the upper and lower division of the central body (CBU and CBL), the protocerebral bridge (PB) and the paired noduli (NO). The medial and lateral bulbs (MBU and LBU) are small neuropils lateral to the central body (CB) and provide the major input to the CBL (Figure 1a,b,d). Based on synapsin staining we divided the CBL into nine vertical slices (Figure 1d). Each nodulus of the paired NO, which are located posteriorly to the CBL, consists of a large upper unit (NOU) and a small lower unit (NOL) (Figure 1e).

Fibers entering or leaving the CX contribute to an ordered arrangement of fiber bundles (Williams, 1975): the ventral groove fiber complex is situated antero-ventrally to the CBL and gives rise to the isthmus tracts, which provide connections between the CX and the lateral complex (LX). The posterior groove fiber complex extends between the CB and the NO (Figure 1c). Midline crossing of fibers occurs either in the posterior chiasma, between the PB and the CB, or via the anterior chiasma of the ventral groove fiber complex.

The LX has been described in different insect species and contains the bulb and the lateral accessory lobe (LAL), which includes the gall (GA). The bulb consists of different subregions that are either largely fused or constitute spatially separated structures depending on species (Ito et al., 2014). The former can be found for example in *Drosophila melanogaster*, where three subregions (superior, inferior, and anterior bulb) form one single structure. The latter holds true for example, for locusts (*Schistocerca gregaria*) but also for *Apis mellifera*, where the two subregions of the bulb (medial bulb (MBU) and lateral bulb (LBU)) are detached from each other. As published previously for the honeybee (Held et al., 2016), MBU and LBU are located ventrolaterally to the CBL (Figure 1a,b,d) and are organized in prominent microglomerular structures. In contrast to MBU and LBU, the GA of the honeybee is poorly visible in synapsin stained preparations. It is defined by the arborizations of columnar neurons of the CBL (CL1 neurons) in the LX. This arborization region can be delimited against surrounding tissue only by its weak staining (Figure 1f). The GA is located in front of the isthmus tract 2 (IT2, Figure 1f), which contains projections of tangential neurons of the CBL (von Hadeln et al., 2020). The largest portion of the LX, the LAL, is situated beneath the medial lobe (ML) of the mushroom body and is flanked antero-ventrally by the antennal lobe (AL), but especially its posterior boundaries are less clearly defined.

Additional regions of the protocerebrum that are strongly connected to the CX, are the superior neuropils, which can be divided into the superior medial protocerebrum (SMP), the superior intermediate protocerebrum (SIP), and the superior lateral protocerebrum (SLP) (Figure 1g). The triangularly shaped neuropil in front of the central body is termed anterior lip (ALI) (Figure 1h).

Neurons are termed according to the nomenclature used in locusts (Heinze & Homberg, 2008; Müller, Homberg, & Kühn, 1997; von Hadeln et al., 2020). Based on their morphology neurons of the CX are conventionally classified into tangential, columnar, pontine, and amacrine neurons. Tangential neurons constitute four subtypes innervating the CBL (TL neurons), the CBU (TU neurons), the PB (TB neurons), or the noduli (TN neurons). Here, we identified five subtypes of TL neuron, nine subtypes of TU neuron, and two subtypes of TN neuron. We did not stain TB neurons, presumably due to the ventral positioning of the injection electrodes. Columnar neurons constitute subtypes with ramifications in the PB and CBL (CL neurons), the PB and CBU (CPU neurons), the PB only (CP neurons), or the CBU only (CU neurons). Here, we describe two subtypes of CL neuron and five subtypes of CPU neuron. Pontine and amacrine neurons connect regions within only one substructure of the CX. Here, we describe one pontine neuron. Amacrine neurons were not stained.

Table 1 and Figure 21 summarize the different types of neuron, including their presumed input and output sites, that were derived from morphological features. Whereas smooth (or fine) processes indicate dendritic structures, varicose (or bleb-like) processes indicate

axonal terminals (e.g., Cardona et al., 2010; Heinze & Homberg, 2009; Wolff et al., 2015).

3.2 | Tangential neurons of the CBL

Extracellular iontophoretic dye injections enabled us to identify four types of tangential neuron (TL1–TL3, TL5) connecting the LX to the CBL and one type of tangential neuron that connects the posterior protocerebrum to the CBL (TL6).

The first type, TL1 (Figure 2), was encountered in six preparations (containing a total of n = 9 TL1 neurons) and comprises at least two cells per hemisphere. Somata of both cells are located medially to the antennal lobe (AL) (Figure 2b, arrows). The primary neurites run laterally, bend posteriorly around the AL and continue via the isthmus tracts toward the CBL (Figure 2a,b). Numerous processes innervate the LAL from anterior to posterior and the GA (Figure 2c, d). Ramifications within the LAL have prominent bleb-like endings and few smooth terminals (Figure 2c,d, arrows and arrowheads, respectively). The neurons enter the CX along the posterior groove and innervate all slices of the CBL (Figure 2e). Ventral regions of the CBL are free from ramifications (Figure 2f,g, asterisks). Three TL1 neurons had arborizations with bleb-like structures in the CBL. For the other TL neurons, the structure of ramifications could not be

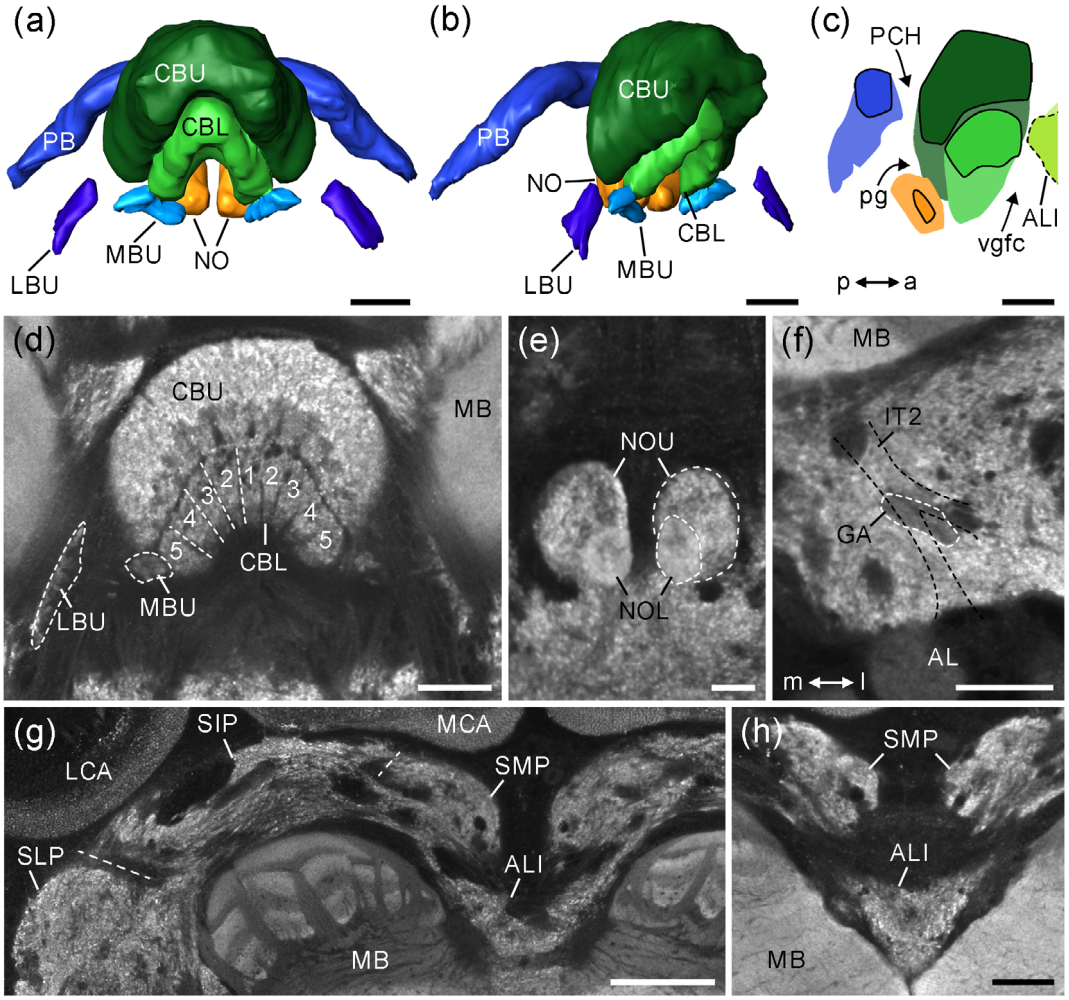

FIGURE 1 Anatomy of the central complex (CX) and associated neuropils. (a) Frontal view of a 3D reconstruction of the CX, the medial bulbs (MBU), and lateral bulbs (LBU) of the lateral complex (LX). (b) Side view of the 3D reconstruction shown in (a). The CX consists of the upper division of the central body (CBU), the lower division of the central body (CBL), the protocerebral bridge (PB), and the paired noduli (NO). (c) Schematic cross section of the 3D reconstruction shown in (a) with indication of the anterior lip (ALI). The posterior groove (pg) extends between the central body and the NO. The posterior chiasma (PCH) is located between the central body and the PB. The ventral groove fiber complex (vgfc) is situated between the CBL and the ALI. (d–h) Optical slices through the CX stained against synapsin. (d) The CBL is divided into nine vertical slices (slice boundaries are indicated by dashed lines for one hemisphere). (e) Each nodulus consists of an upper unit (NOU) and a lower unit (NOL). (f) The gall (GA), a small elongated neuropil within the LX, is located anterior to the isthmus tract 2 (IT2; boundaries indicated by black dashed lines). (g) Appearance of superior neuropils in an optical slice anterior to the CX (boundaries are indicated by dashed lines). (h) The anterior lip (ALI) is located anterior to the central body. a, anterior; l, lateral; LCA, lateral calyx of the mushroom body; MB, mushroom body; MCA, medial calyx of the mushroom body; m, medial; p, posterior; SIP, superior intermediate protocerebrum; SLP, superior lateral protocerebrum; SMP, superior medial protocerebrum. Scale bars = 50 μm (a–d,f,h), 20 μm (e), 100 μm (g) [Color figure can be viewed at wileyonlinelibrary.com]

TABLE 1 Types of neuron in the honeybee central complex and their regions of arborization

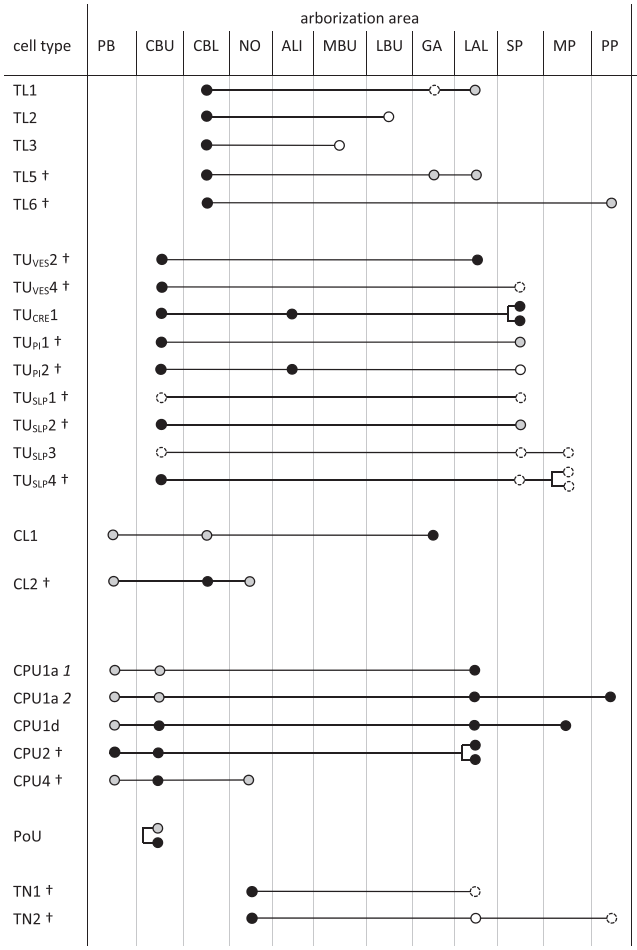

Note: Black circles, varicose, or bleb-like arborizations; open circles, smooth or fine arborizations; gray circles, mixed arborizations; circles with dashed outline, undefined structure of arborizations.

Abbreviations: ALI, anterior lip; CBL, lower division of the central body; CBU, upper division of the central body; GA, gall; LAL, lateral accessory lobe; LBU, lateral bulb; MBU, medial bulb; MP, medial protocerebrum; NO, noduli; PB, protocerebral bridge; PP, posterior protocerebrum; SP, superior protocerebrum. "†" denotes types of neuron that are described for the first time in the honeybee. "‡" denotes the neuron could be homologues to either CPU1a *Type 1* or CPU1d.

determined, because additional neurons were labeled or the staining was too faint.

Two types of TL neuron (TL2 and TL3) have been described previously (Held et al., 2016). As in the locust (Müller et al., 1997; Träger, Wagner, Bausenwein, & Homberg, 2008) their dendritic endings are part of the microglomerular complexes of the LBU (TL2) and MBU (TL3) in the LX. Here, we provide further detail on their morphological characteristics. TL2 neurons (Figure 3) were found in eight preparations, each containing up to five TL2 neurons per hemisphere. TL2 neurons have their cell bodies along the dorso-posterior boundary of the AL and send their primary neurites via the isthmus tracts through the LX. In the LBU, most TL2 neurons have one prominent stalk-like side branch with a tuft-like ending (Figure 3a–c). Only few TL2 neurons lack a prominent stalk or have less compact endings (Figure 3c, arrow). Neurites continue toward the CBL where they ramify in one layer, which covers the anterior-most region and the ventral part of more posterior regions of the CBL (Figure 3d–g). In most preparations scattered ramifications extend into the space between those extensively innervated areas (data not shown).

TL3 neurons were found in 10 preparations. The morphology of TL3 neurons (Figure 4) resembles that of TL2 neurons with respect to cell body position and course of the primary neurite. In contrast to TL2 neurons, TL3 neurons ramify in the MBU, where the main fibers give rise to few short processes that terminate in dense tufts of fine endings (Figure 4a–c). Axons extend toward the CBL and give off branches into all slices as they continue along its ventral concavity (Figure 4d). Ventral regions of the CBL are not innervated (Figure 4e–g), indicating that TL2 and TL3 neurons have complementary arborization areas within this neuropil.

A fourth type of TL neuron (TL5, Figure 5) was encountered in four preparations. In all four preparations only a single TL5 neuron was stained together with other neuronal cell types. In contrast to TL neurons outlined above, TL5 neurons have their cell bodies in the

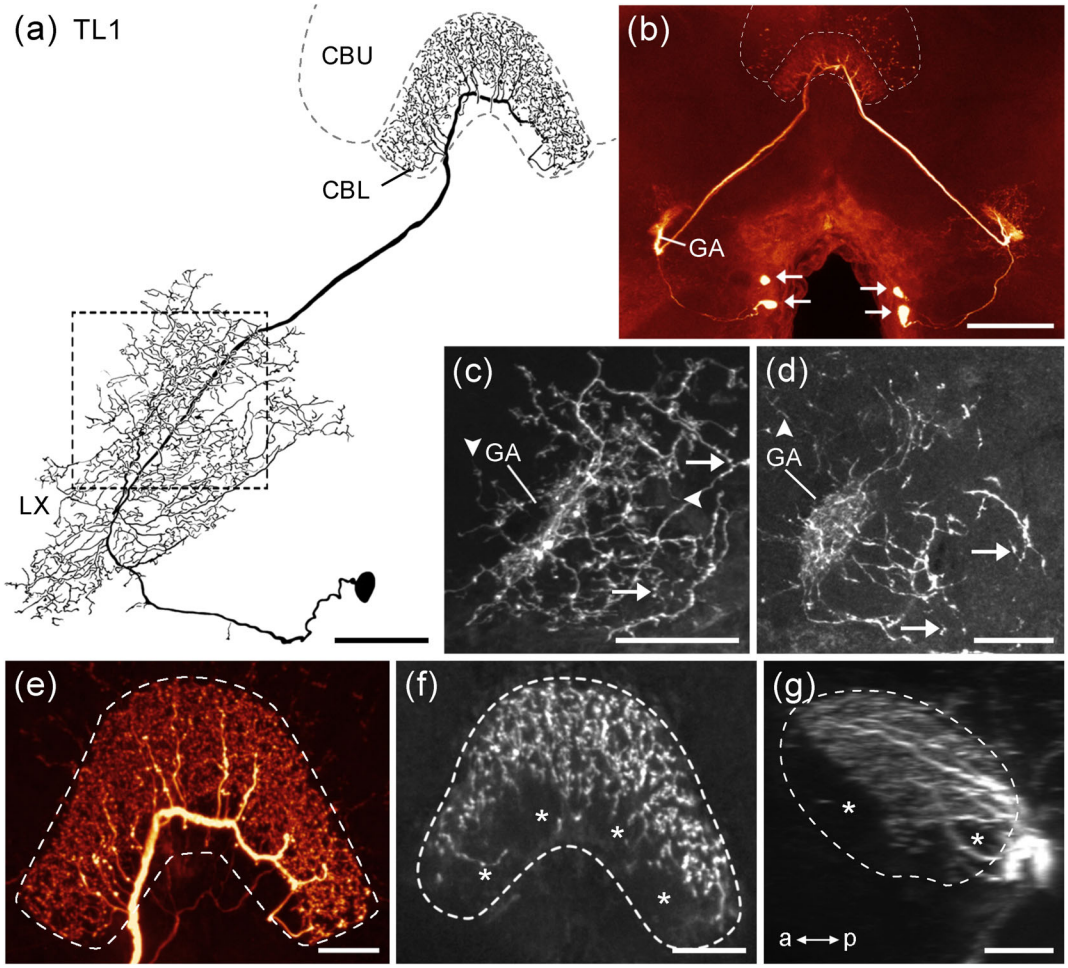

FIGURE 2 Tangential neurons of the lower division of the central body (CBL), the lateral accessory lobe (LAL) and the gall (GA). (a) Reconstruction of a TL1 neuron. Its cell body is located medial to the AL. Outlined rectangle: area shown in (c). (b) Maximum intensity visualization of four TL1 neurons in one preparation. This cell type comprises at least two cells per hemisphere (arrows). (c) Maximum intensity visualization of 30 optical slices depicting mixed terminals within the LAL and the GA of the TL1 neuron shown in (a). Arrows indicate bleb-like endings. Arrowheads point to smooth terminals. (d) Maximum intensity visualization of 10 optical slices depicting mixed terminals of another TL1 neuron within the LAL and the GA. Arrows indicate bleb-like endings. The arrowhead points to smooth terminals. (e) Maximum intensity visualization of varicose branches of the TL1 neuron shown in (a) in all slices of the CBL. (f) Maximum intensity visualization of 10 optical slices depicting the branches of the TL1 neuron in the CBL. Ventral regions of the CBL are free from ramifications (asterisks). (g) Sagittal view of a maximum intensity visualization of optical slices in the center of the CBL. Ventral regions are free from ramifications (asterisks). CBU, upper division of the central body. Scale bars = 50 μm (a), 100 μm (b), 40 μm (c), 20 μm (d-g) [Color figure can be viewed at wileyonlinelibrary.com]

lateral pars intercerebralis (PI) posterior to the PB. Their primary neurite bends around the PB and runs ventrally toward the isthmus tracts where it splits up into several fibers. Two of them project into the ipsilateral LX and innervate the GA and surrounding areas within the LAL (Figure 5a,b). Ramifications appear smooth with only scattered bleb-like structures. Due to staining of additional neurons in the same preparation we could not unambiguously assign all processes to the TL5 neuron (Figure 5b, asterisks). The other fiber runs dorsomedially. Ventral to the CBL near the brain midline, it gives rise to several processes that enter the CBL (Figure 5a,c). Bleb-like terminals appear in all slices but could not be discriminated unambiguously from arborizations of other TL neurons (Figure 5c). In one preparation a TL1, a TL3 and a TL5 neuron were colabeled. Although details of processes could not be assigned to each individual neuron, 3D reconstruction of their major neurites indicates that they ramify at least partly in similar regions of the CBL (Figure 5d–f). The main neurite of the TL1 neuron runs along the posterior groove, whereas that of the TL3 neuron crosses the midline of the brain more anteriorly. The neurite of the TL5 neuron branches conspicuously ventrally to the CBL.

One selective Neurobiotin fill and colabeling in two other preparations (n = 3) revealed a TL neuron that has not been described in other species and is termed here TL6 neuron (Figure 6). It differs markedly from other TL neurons. The cell body of the neuron resides in the lateral PI close to cell bodies of TL5 neurons. The primary neurite projects medially along the ventral border of the PB and splits into two branches posterior-lateral to the CBU (Figure 6a). One branch runs ventrally and gives rise to a large arborization area, with

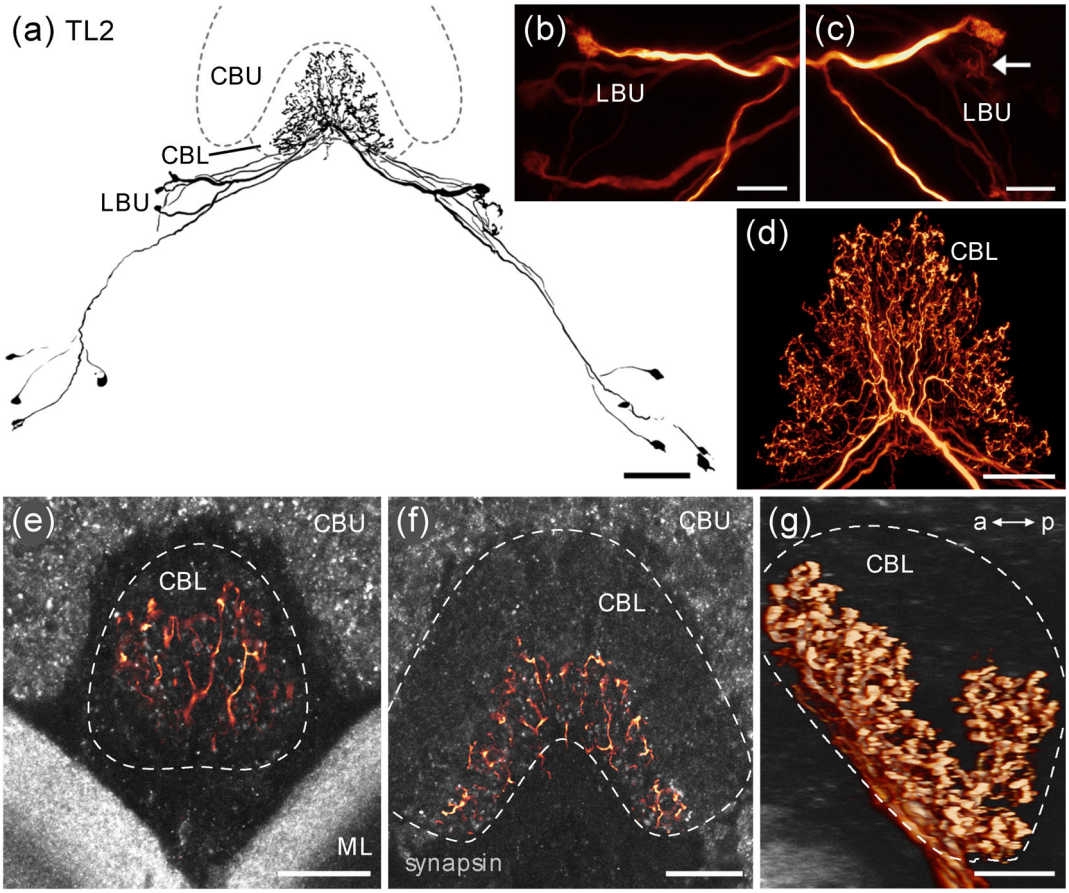

FIGURE 3 Tangential neurons of the CBL and the lateral bulb (LBU). (a) Reconstruction of nine TL2 neurons. (b,c) Maximum intensity visualization of endings in the LBU of the neurons shown in (a). One stalk-like side branch originates from the main neurite and terminates in a tuft of fine processes. Some neurons possess less compact tufts (c, arrow). (d) Maximum intensity visualization of arborizations of TL2 neurons shown in (a) in the CBL. (e,f) Single optical slices of arborizations of TL2 neurons shown in (a) in the CBL. Neurons are shown in orange, and neuropils (anti-synapsin staining) are shown in gray. Anterior regions of the CBL are innervated (e), only ventral regions of the posterior CBL are innervated (f). (g) Sagittal view of a 3D visualization (volume rendering) of the arborizations shown in (d–f) (orange colors). Neuropil background (anti-synapsin staining) is shown in gray. An anterior-ventral band, spanning the CBL from its anterior tip to posterior-ventral regions, is innervated by the neurons. CBU, upper division of the central body; a, anterior; p, posterior. Scale bars = 50 μm (a), 10 μm (b,c), 20 μm (d–g) [Color figure can be viewed at wileyonlinelibrary.com]

intermingled bleb-like and smooth processes, within the posterior slope (Figure 6b). The other branch projects dorsally. It gives off three processes that bend around the anterior surface of the CBU and reach into the CBL. Except for a narrow ventral band the whole CBL is filled with varicose processes (Figure 6c,d). Additionally, a few bleb-like processes spread into a small area in close proximity to the MBU (Figure 6d, arrow).

3.3 | Columnar neurons of the CBL

Columnar neurons of the CBL connect individual slices of the PB and the CBL to the contralateral GA (CL1 neurons) or nodulus (CL2 neurons). We encountered CL1 neurons in thirteen preparations. They have cell bodies in the PI and innervate slice 1 of the CBL (n = 7), slice 2 of the CBL (Figure 7a–c′, n = 8), slice 3 of the CBL (n = 3), or slice 4 of the CBL (Figure 7g–i′, n = 1). We did not label CL1 neurons that innervate the outermost slices of the CBL.

The general morphology of CL1 neurons (Figure 7) was highly similar in all preparations. Their primary neurites run anteriorly toward the PB where they ramify in one ipsilateral slice. Arborizations of CL1 neurons in the PB consist of similar proportions of bleb-like and fine structures (Figure 7b′, arrows and arrowheads, respectively). From the PB neurites continue toward the CBL and give off processes covering single slices (Figure 7a,g). CL1 neurons with contralateral CBL and GA arborizations cross the midline of the brain in the posterior chiasma (between PB and CBU). CL1 neurons with ipsilateral CBL arborizations and contralateral GA arborizations cross the midline of the brain in the anterior chiasma (between CBL and ALI). Staining of a single CL1 neuron revealed intermingled bleb-like and smooth ramifications in the CBL (Figure 7c′, arrows and arrowheads, respectively). In contrast to the different types of TL neuron CL1 neurons appear to innervate all layers within one slice (Figure 7d,e). From the CBL their

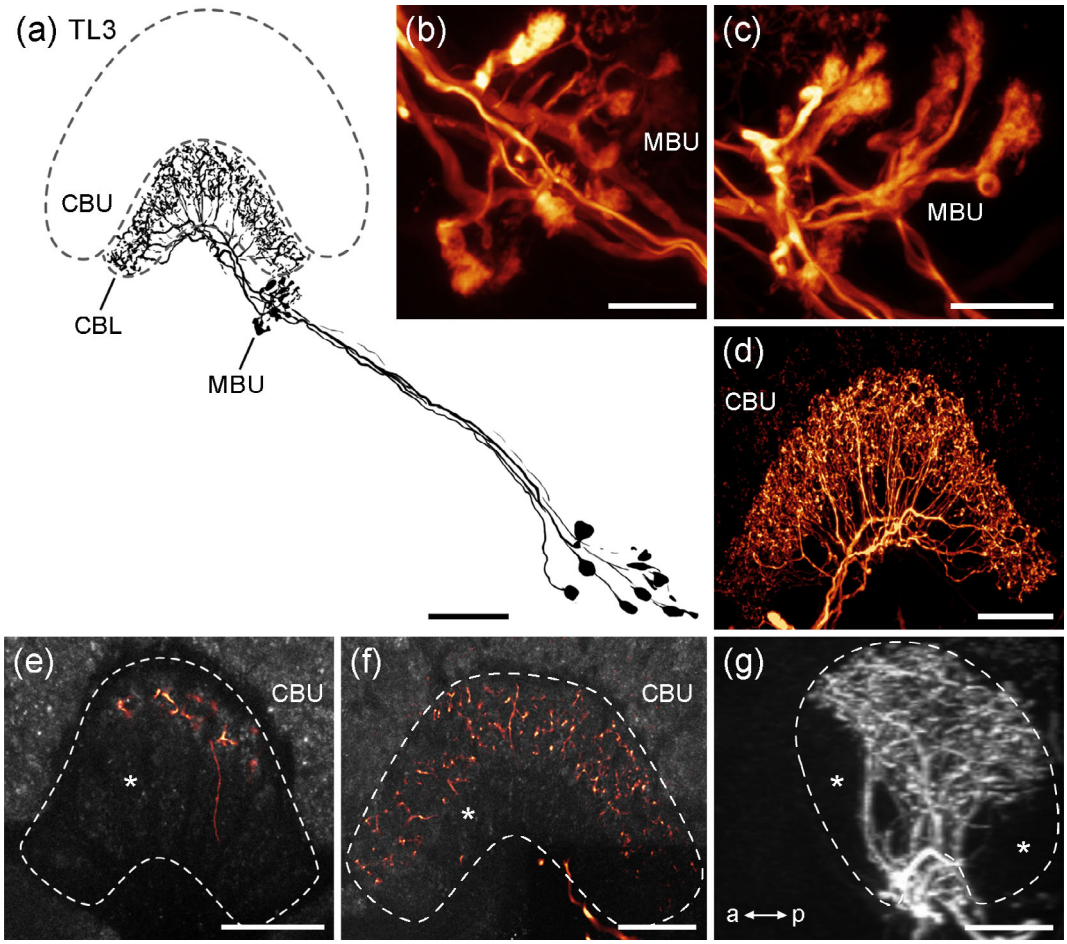

FIGURE 4 Tangential neurons of the CBL and the medial bulb (MBU). (a) Reconstruction of several TL3 neurons in one preparation. (b) Maximum intensity visualization of endings in the MBU of TL3 neurons shown in (a). Thin processes extend from the main neurite of each neuron and terminate in tufts of fine endings. (c) Maximum intensity visualization of branches within the MBU of TL3 neurons stained in another preparation. (d) Maximum intensity visualization of arborizations in the CBL of TL3 neurons shown in (a). TL3 neurons innervate all slices of the CBL. (e,f) Single optical slices of arborizations within the CBL. Neurons are shown in orange, neuropils (anti-synapsin staining) are shown in gray. TL3 neurons do not arborize in ventral regions of the CBL (asterisks). (g) Sagittal view of a maximum intensity visualization of optical slices in the center of the CBL. Ventral regions are free from ramifications (asterisks). CBU, upper division of the central body. Scale bars = 50 μm (a), 20 μm (b,g), 10 μm (c), 25 μm (d,e,f) [Color figure can be viewed at wileyonlinelibrary.com]

neurites continue to the contralateral GA. Terminals in the GA are always characterized by large bleb-like structures (Figure 7f,j). Only one CL1 neuron differs from the others regarding the appearance of its terminals (Figure 7g–i′). Its ramifications in the PB and CBL are mainly bleb-like. In contrast, terminals of the other CL1 neurons display similar amounts of bleb-like and fine endings. Additionally, PB and CBL seem to be more densely innervated by this CL1 neuron and in the GA it covers a smaller area than other CL1 neurons do.

Neurobiotin injections led to labeling of CL2 neurons in three preparations. Cell bodies of CL2 neurons are located in the PI (Figure 8). Their primary neurites project anteriorly and give off side branches that innervate one slice of the PB. Processes within the PB exhibit bleb-like as well as smooth endings (Figure 8b,b′, arrows and arrowheads, respectively). The neurites leave the PB from its anterior surface and run medially between PB and CBU toward the CBL. From the CBL they turn posteriorly toward the contralateral nodulus. Midline crossing of CL2 neurites occurs in either the posterior chiasma (for contralateral CBL projections) or in the posterior groove (for ipsilateral CBL projections). Arborizations in the CBL span the width of one slice and have a bleb-like appearance (Figure 8a,c,d). Similar to ramifications of TL1, TL3, and TL6 neurons they omit ventral regions of the CBL (Figure 8d). Within the NO, CL2 neurons have mixed terminals that are confined to the lower unit of one nodulus (NOL, Figure 8e,f).

3.4 | Columnar neurons of the CBU

Three types of columnar neuron of the CBU were stained: CPU1, CPU2, and CPU4 neurons (Figures 9–12). Some of these could be further categorized, resulting in a total of five morphologically identifiable subtypes of CPU neuron.

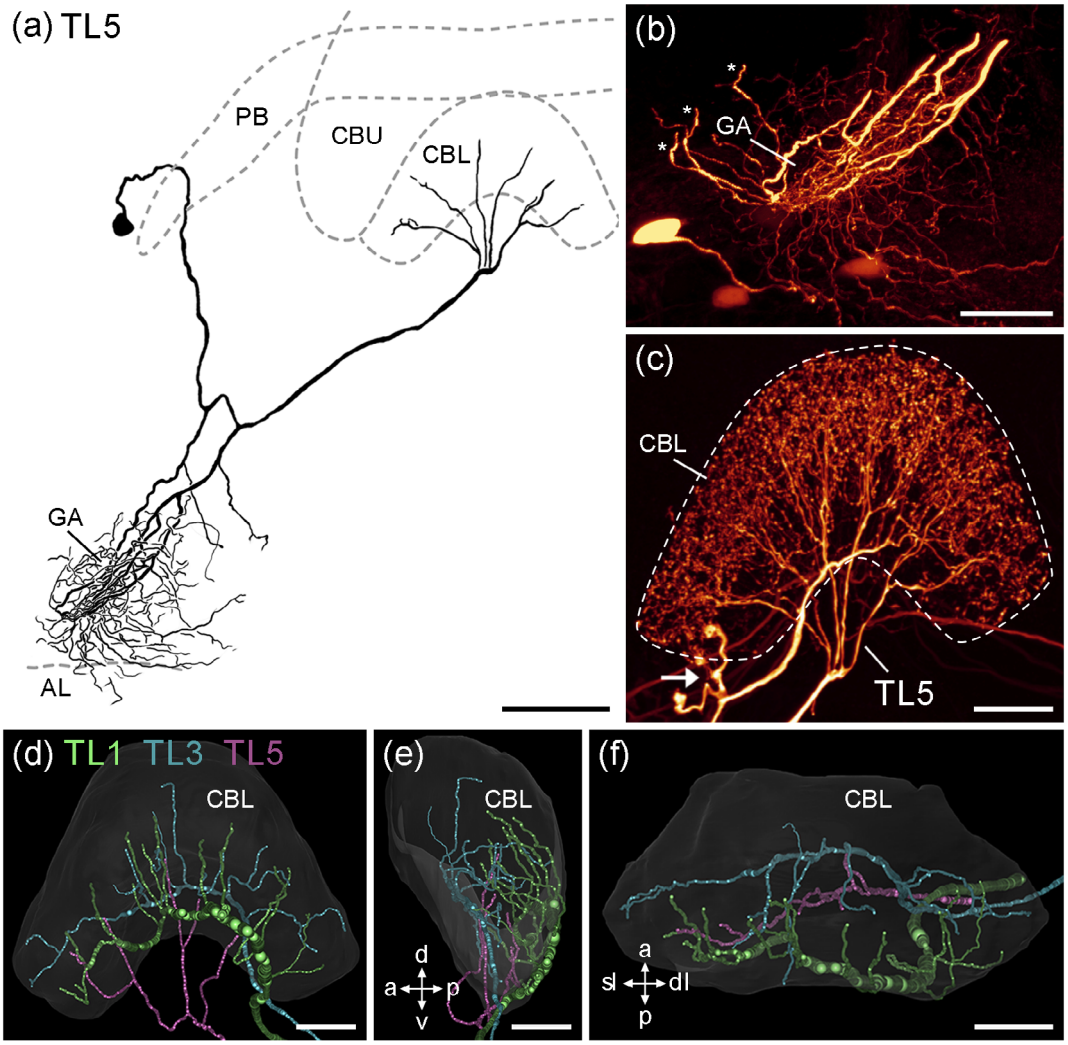

FIGURE 5 Tangential neuron of the CBL and the lateral complex (LX) with cell body in the lateral pars intercerebralis. (a) Reconstruction of a TL5 neuron. The neuron arborizes in the lateral accessory lobe (LAL), the gall (GA), and the CBL. Arborizations in the CBL could not be traced completely, as the neuron was labeled together with a TL3 neuron (c, arrow). (b) Maximum intensity visualization of smooth branches of the TL5 neuron shown in (a) in the LX. Staining of additional neurons prevented us from assigning all arborizations to the TL5 neuron (asterisks). (c) Maximum intensity visualization of varicose arborizations of the TL5 neuron shown in (a) and a TL3 neuron (arrow) in the CBL. (d–f) 3D reconstruction of the major neurites of a TL1 (green), a TL3 (blue), and a TL5 (purple) neuron projecting into the CBL. Details of processes of each neuron could not be traced. (d) Frontal view. (e) Sagittal view. (f) Horizontal view. TL1 neurons enter the CBL from the posterior groove. TL3 neurons enter the CBL more anterior along its ventral concavity. TL5 neurons show a characteristic branching point located more ventrally to the CBL. AL, antennal lobe; CBU, upper division of the central body; PB, protocerebral bridge; a, anterior; dl, dextro lateral; d, dorsal; p, posterior; sl, sinistro lateral; v, ventral. Scale bars = 50 μm (a), 20 μm (b–f) [Color figure can be viewed at wileyonlinelibrary.com]

Three subtypes of CPU1 neuron connect the PB and CBU to the contralateral medial protocerebrum (Figures 9 and 10). Midline crossing occurs in either the posterior chiasma (for contralateral CBU projections) or in the anterior chiasma (for ipsilateral CBU projections). Single CPU1a *Type 2* neurons (Figure 9a–d) were encountered in three preparations, of which one also contained a CPU1a *Type 1* neuron (Figure 9e–g′). CPU1a neurons have their cell bodies in the posterior PI and project anteriorly to the PB. In the PB ramifications of the CPU1a *Type 2* neuron are confined to one slice (Figure 9a–b′). Whether CPU1a *Type 1* neurons innervate one PB slice or two neighboring slices could not be determined (Figure 9e,f,f′). PB arborizations of both types consist of mainly smooth structures (Figure 9b,b′,f,f′) and only few bleb-like regions (Figure 9b′, arrows). From the PB neurites continue anterior-medially and send processes into distinct regions of the CBU: Ramifications of CPU1a *Type 2* neurons span the width of one slice (Figure 9g, arrowheads), whereas ramifications of CPU1a *Type 1* neurons occupy the width of two slices (Figure 9g, arrows). Both types innervate the posterior CBU but occupy either ventral (CPU1a *Type 2*) or dorsal regions (CPU1a *Type 1*). Processes appear smooth with scattered bleb-like regions (Figure 9c′g', arrows). From the CBU neurites of CPU1a neurons run in parallel to the LX, where they give off several side branches with varicose endings. Neurites of CPU1a *Type 2* neurons turn further posterior and innervate the posterior lateral protocerebrum (Figure 9e,h,i, arrowheads).

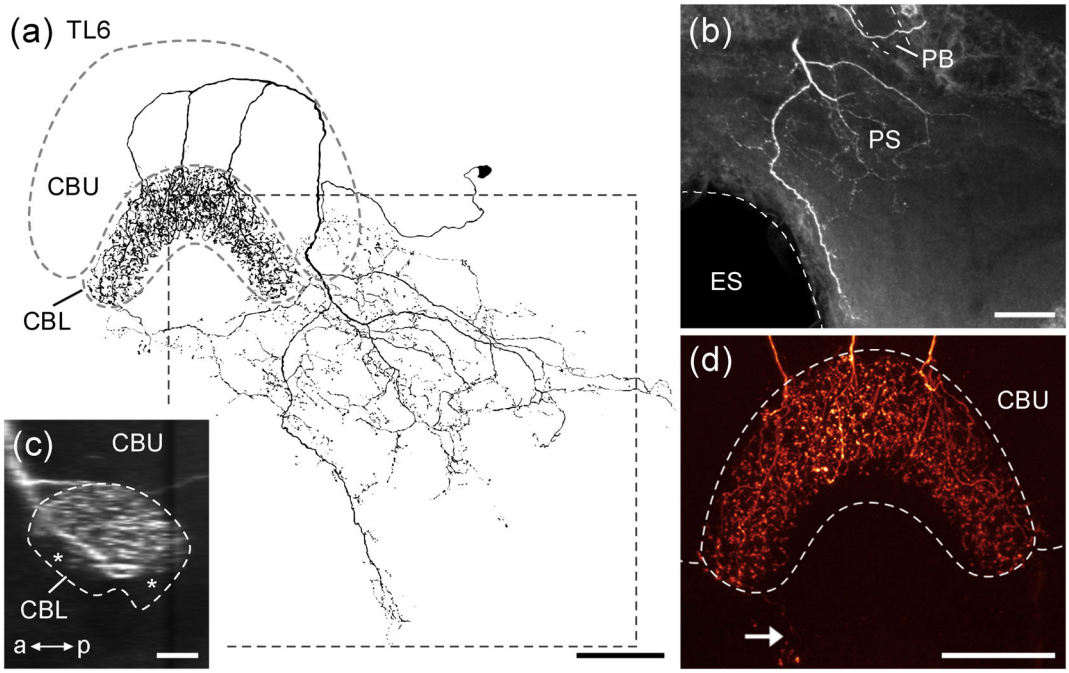

FIGURE 6 Tangential neuron of the CBL and the posterior protocerebrum. (a) Reconstruction of a TL6 neuron with cell body in the lateral pars intercerebralis. Outlined rectangle: area shown in (b). (b) Maximum intensity projection of 100 optical slices depicting bleb-like and smooth terminals of the TL6 neuron in the posterior slope (PS). (c) Sagittal view of a maximum intensity visualization of optical slices in the center of the CBL. Ventral regions are free from ramifications (asterisks). (d) Maximum intensity visualization of varicose arborizations of the TL6 neuron in the CBL. Few bleb-like endings extend ventrally (arrow). CBU, upper division of the central body; PB, protocerebral bridge. Scale bars = 50 μm (a,b), 20 μm (c), 40 μm (d) [Color figure can be viewed at wileyonlinelibrary.com]

Arborizations of CPU1a *Type 1* neurons extend more medially and anteriorly than those of CPU1a *Type 2* neurons (Figure 9e,i, arrow).

The third type of CPU1 neuron was stained in three preparations. Because its connectivity scheme did not fit that of CPU1b or CPU1c neurons described in the locust (Heinze & Homberg, 2008) we termed this type of neuron CPU1d neuron. Similar to CPU1a neurons, CPU1d neurons have their somata in the posterior PI and arborize within single slices of the PB (Figure 10a,b). CPU1d neurons possess a broad area of arborizations within the CBU. Nevertheless, due to faint staining (Figure 10a) in two preparations and colabeling of several CPU1 neurons in one preparation (Figure 10b–e) ramifications within the CBU could not be analyzed in more detail. From the CBU CPU1d neurons project toward the LX and terminate ventral and medial to the vertical lobe (VL) of the mushroom body (Figure 10d,e). The most striking difference between CPU1d and CPU1a neurons is the appearance of these terminals. Although, similar to CPU1a neurons, CPU1d neurons have varicose terminals in the LX, they are different in that they occur as local accumulations that form microglomeruli-like structures.

In addition to CPU1 neurons, we encountered CPU2 neurons (n = 2) that connect the PB and CBU to the LX of both brain hemispheres (Figure 11). In contrast to CPU1 neurons, CPU2 neurons have their cell body in the anterior PI. Their primary neurite projects posteriorly toward the anterior surface of the PB and sends processes into one slice (Figure 11b,b′). The main neurite turns back anteriorly to the CBU. It crosses the midline of the brain and gives off processes that branch in the posterior CBU around the brain midline (Figure 11a,c). Processes in the PB appear mixed, whereas the CBU contains mainly bleb-like specializations. From the CBU the neurons project ventrally and bifurcate posterior to the anterior lip. Each of the emerging axons continues via the isthmus tracts toward the LX of one brain hemisphere. Here, it terminates in bleb-like structures (Figure 11d,e).

Another subtype of CPU neuron connects the PB and the CBU to the contralateral nodulus (CPU4 neurons, Figure 12). CPU4 neurons have cell bodies in the posterior PI (Figure 12a,e). Their primary neurites project anteriorly and give off mixed terminals into single slices of the PB. From the PB neurites continue toward the CBU (Figure 12a,c,e,g). In one preparation (Figure 12a–d), arborizations within the CBU possess several bleb-like regions but barely branch out (Figure 12c). In another preparation, in which at least five CPU4 neurons were labeled (Figure 12e–h′), the bleb-like structure of endings is much more prominent (Figure 12g). One neurite of each CPU4 neuron continues toward the contralateral nodulus, where it gives rise to mixed endings (Figure 12d) or predominantly bleb-like terminals (Figure 12h). Arborizations omit the NOL (Figures 12d, asterisk and 12h′) and are restricted to distinct regions within the NOU.

3.5 | Pontine neurons of the CBU

In one preparation injection of Neurobiotin led to staining of a single pontine neuron (PoU, Figure 13) that interconnects different slices

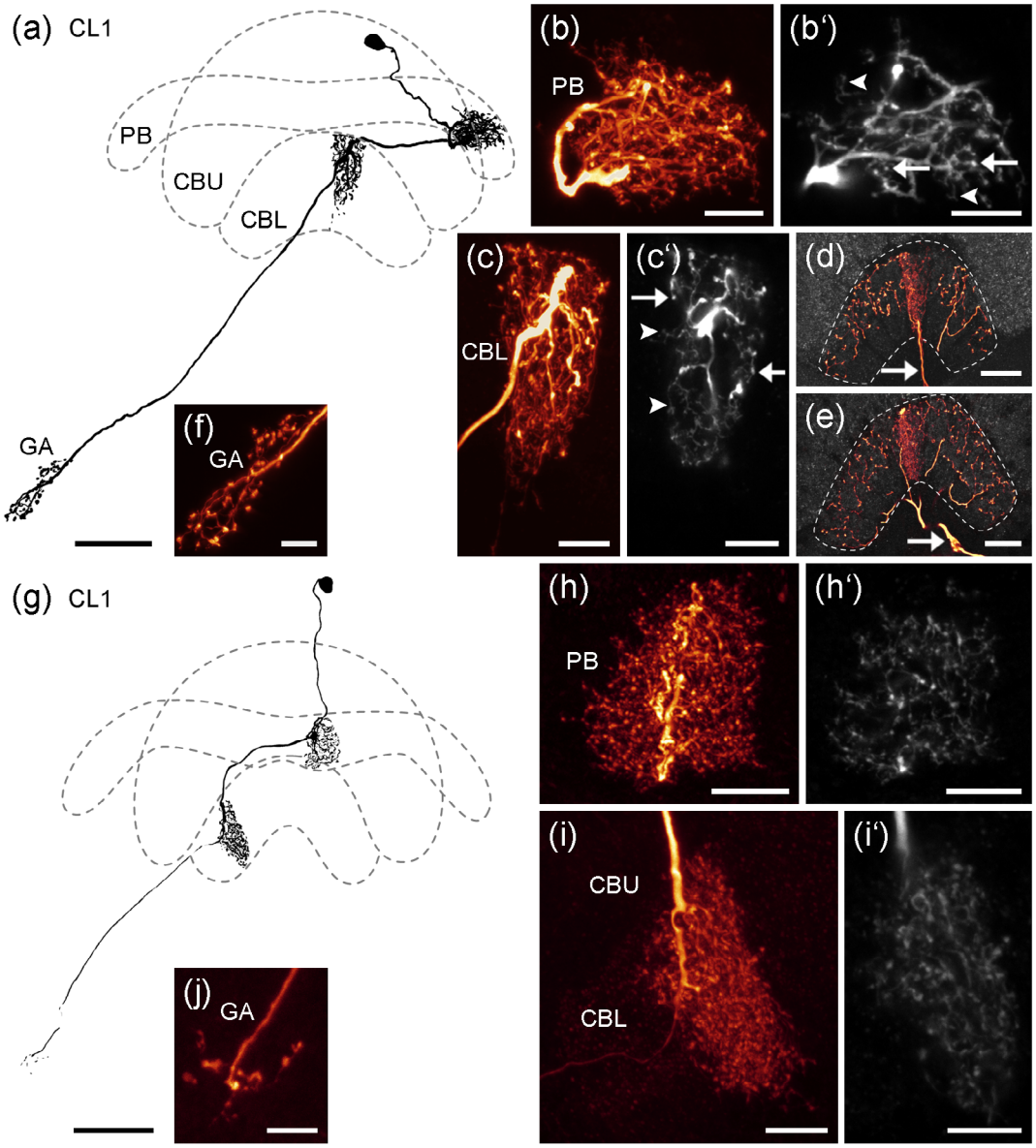

FIGURE 7 Columnar neurons of the protocerebral bridge (PB) and the lower division of the central body (CBL) with arborizations in the gall (GA). (a) Reconstruction of a CL1 neuron. (b,b′) Maximum intensity visualization of the whole arborization tree of the CL1 neuron in the PB (b) or of 10 optical slices (b′). Ramifications in the PB show intermingled bleb-like (arrows) and smooth (arrowheads) endings. (c,c′) Maximum intensity visualization of the whole arborization tree in the CBL (c) and of 10 optical slices (c′). The neuron innervates one slice. Ventral regions of the CBL are only sparsely innervated. The CL1 neuron possesses varicose (arrows) and smooth (arrowheads) arborizations in the CBL. (d,e) Maximum intensity visualization of a CL1 neuron and a TL3 neuron (arrow) in the anterior (d) and the posterior (e) CBL. Neurons are shown in orange and neuropils (anti-synapsin staining) in gray. While arborizations of the TL3 neuron omit ventral regions, the CL1 neuron innervates all regions within one slice. (f) Maximum intensity visualization of bleb-like arborizations of the CL1 neuron in the GA. (g) Reconstruction of a CL1 neuron with arborizations in the contralateral CBL. (h, h′) Ramifications in the PB exhibit predominantly bleb-like endings. (i,i′) The arborization tree of the CL1 neuron shown in (g) in the CBL is densely packed and is dominated by bleb-like structures. (j) Arborizations of the same CL1 neuron in the GA show some bleb-like structures, but appear sparse. CBU, upper division of the central body. Scale bars = 50 μm (a,g), 10 μm (b–c′,f,h,h′), 20 μm (d,e,i,i′) 5 μm (j) [Color figure can be viewed at wileyonlinelibrary.com]

within the CBU. The cell body is located in the PI. The primary neurite runs ventrally toward the PB. From here, it turns anteriorly along the dorsal surface of the CBU. Several fine processes split off. They proceed further anterior and densely innervate slices at and adjacent to the brain midline in the anterior CBU (Figure 13b). Ramifications are smooth, but appear as fine granular structures in some regions. The main neurite continues toward the outermost contralateral region of the CBU, where it splits into several side branches with bleb-like terminals (Figure 13c). Arborizations are restricted to anterior regions of the CBU.

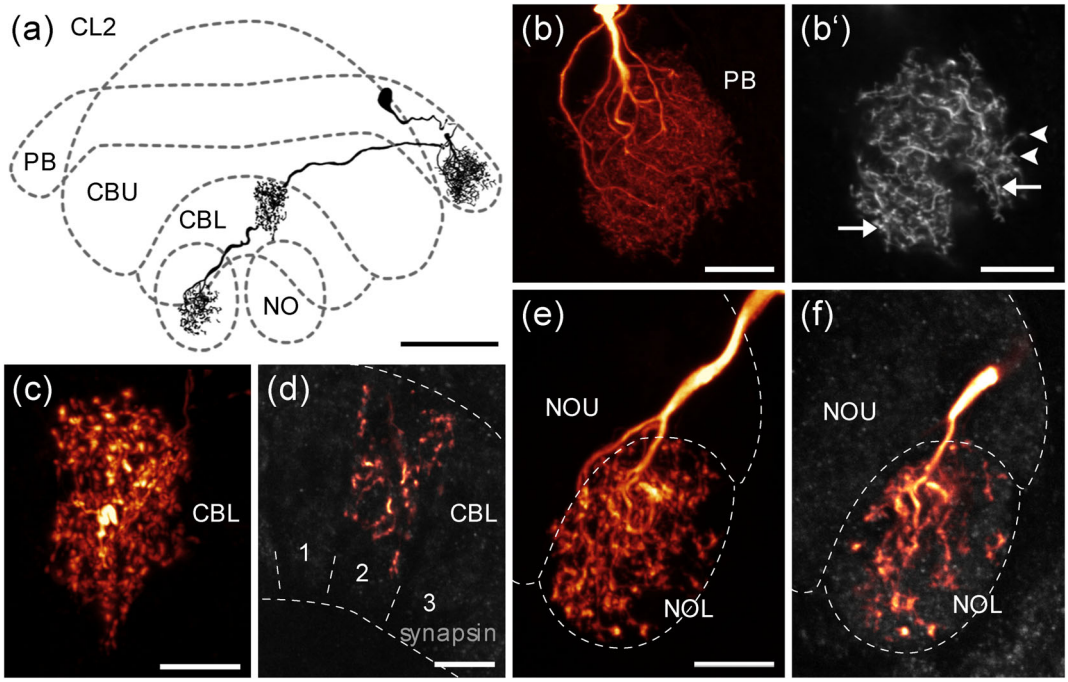

FIGURE 8 Columnar neurons of the protocerebral bridge (PB) and the lower division of the central body (CBL) with arborizations in the contralateral nodulus. (a) Reconstruction of a CL2 neuron. The cell body is located in the pars intercerebralis. (b,c) Maximum intensity visualization of the arborization trees of the CL2 neuron in the PB (b,b′ [two optical slices]) and the CBL (c). Arborizations in the PB exhibit smooth (arrowheads) and bleb-like (arrows) structures, whereas pronounced bleb-like endings are found in the CBL. (d) The CL2 neuron (orange) innervates one slice of the CBL. Ramifications are mainly restricted to dorsal regions. Neuropils (anti-synapsin staining) are shown in gray. (e,f) Maximum intensity visualization of arborizations in the contralateral nodulus. Neuropils (anti-synapsin staining) are shown in gray (f). The CL2 neuron innervates only the lower unit (NOL) of the contralateral nodulus. The structure of ramifications appears mixed. CBU, upper division of the central body; NOU, upper unit of the nodulus. Scale bars = 50 μm (a), 10 μm (b–f) [Color figure can be viewed at wileyonlinelibrary.com]

3.6 | Tangential neurons of the CBU

Tangential neurons that connect different regions of the protocerebrum to all slices of the CBU are termed TU neurons. We encountered nine types of TU neuron (Figure 21), which were grouped according to their soma position and named after a prominent neuropil next to their soma.

Three types of TU neuron with somata in the ventral protocerebrum medial to the AL were labeled ($TU_{VES}2$, n = 1, $TU_{VES}4$ n = 1, and $TU_{CRE}1$, n = 1). The primary neurites of the $TU_{VES}2$ neuron (Figure 14a–c) and the $TU_{VES}4$ neuron (Figure 14d–f) project dorso-laterally toward the LX. Here, the $TU_{VES}2$ gives off several side branches that possess predominantly bleb-like endings (Figure 14b). Simultaneous staining of a CL1 neuron shows that ramifications of the $TU_{VES}2$ neuron are located mainly posterior to the GA. Only few endings were found close to the GA (Figure 14b′, arrows). Neurites of the $TU_{VES}2$ and $TU_{VES}4$ neuron continue via the isthmus tracts toward the CX. Ventral to the CBL the neurite of the $TU_{VES}2$ neuron splits up and innervates posterior-ventral regions of all slices of the CBU (Figure 14c). Terminals within this area possess predominantly bleb-like specializations (Figure 14c, arrows). Anterior regions of the CBU are free from arborizations. The primary neurite of the $TU_{VES}4$ neuron bifurcates anteriorly to the ipsilateral side of CBL (Figure 14d). One of the resulting branches runs ventrally toward the brain midline and splits up into three side branches that project dorsally and innervate anterior regions of the CBU with bleb-like terminals (Figure 14e). The other branch runs dorso-laterally and splits up within the superior intermediate protocerebrum (SIP) (Figure 14f, arrow). Owing to staining of additional neurons within the preparation (Figure 14e,f, arrowheads), not all processes within the CBU and especially the SIP could be identified.

The soma of the $TU_{CRE}1$ neuron is located superior to the AL (Figure 15a). Different from somata of TU_{VES} neurons it is located near the anterior surface of the brain. Its primary neurite passes the ML anteriorly and projects toward the CX. Medial to the VL the primary neurite splits up into three thick branches (1–3, Figure 15a) of which the dorsalmost (1, Figure 15a,b) runs dorso-laterally and gives rise to ramifications within the ipsilateral superior protocerebrum (Figure 15b). The central branch (2, Figure 15a) continues toward the brain midline and splits into several side branches that innervate the anterior CBU (Figure 15c,d). The third branch (3, Figure 15a,b) bifurcates anteriorly to the anterior lip (ALI) and sends one side branch into the superior protocerebrum of each brain hemisphere. Within the superior protocerebrum innervations have bleb-like terminals and are most abundant in the SIP. Only few processes extend into the superior medial protocerebrum (SMP). Processes within the CBU appear

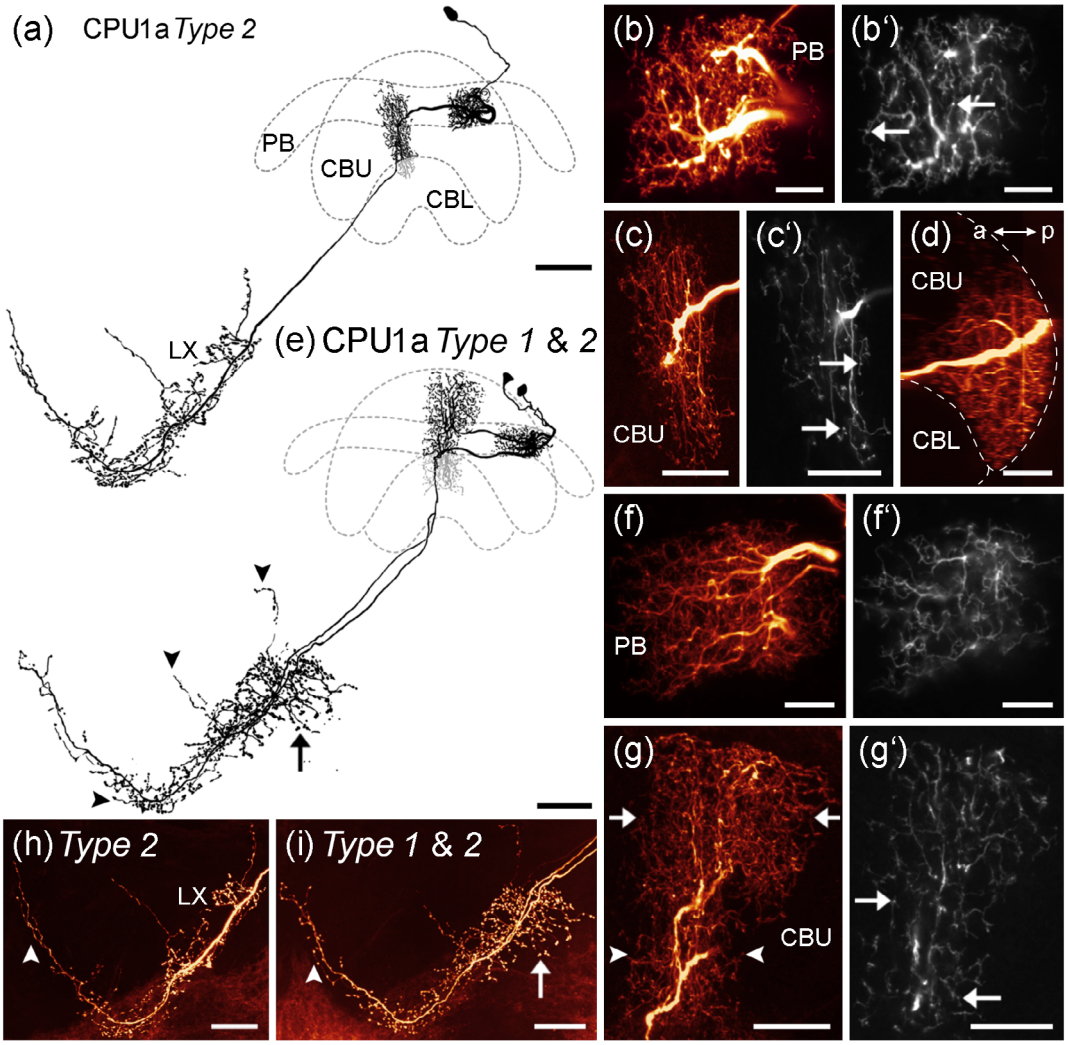

FIGURE 9 Columnar neurons of the protocerebral bridge (PB) and the upper division of the central body (CBU) with arborizations in the contralateral lateral complex (LX) and the posterior lateral protocerebrum. (a) Reconstruction of a CPU1a *Type 2* neuron. Note that arborizations depicted in gray are not in the CBL but in a ventral region of the CBU that extends posteriorly to the CBL (see (d)). (b–c′) Maximum intensity visualization of the whole arborization tree of the CPU1a *Type 2* neuron in the PB (b) and the CBU (c) and of five optical slices of these regions (b′,c′). The CPU1a *Type 2* neuron ramifies within one slice of the PB and the CBU. Terminals in both neuropils appear predominantly smooth, with only a few bleb-like structures (b′,c′, arrows). (d) Sagittal view of a maximum intensity visualization of the arborizations in the CBU. Ramifications are restricted to a ventro-posterior region of the CBU. (e) Reconstruction of a CPU1a *Type 1* and a CPU1a *Type 2* neuron in the same preparation. Note that arborizations depicted in gray are not in the CBL but in a ventral region of the CBU that extends posteriorly to the CBL. Arrowheads point to arborizations of the CPU1a *Type 2* neuron in the LX, whereas the arrow indicates ramifications of the CPU1a *Type 1* neuron. (f–g′) Maximum intensity visualization of the whole arborization tree of both neurons in the PB (f) and the CBU (g) and of five optical slices of these regions (f′,g′). Smooth arborizations in the PB cover a width broader than one slice. Whereas the CPU1a *Type 2* neuron ramifies within one ventral slice of the CBU (g, arrowheads), the CPU1a *Type 1* neuron occupies dorsal regions of the CBU across a width of two slices (g, arrows). Arborizations in the CBU are predominantly smooth, with only a few bleb-like endings (g′, arrows). (h,i) Maximum intensity visualization of bleb-like arborizations in the LX of the neuron shown in (a) and the two neurons shown in (e), respectively. CPU1a *Type 2* neurons show characteristic arborizations that extend posteriorly into the lateral protocerebrum (arrowheads), whereas those of CPU1a *Type 1* neurons remain restricted to the LX, where they occupy a larger area than CPU1a *Type 2* neurons (arrow). CBL, lower division of the central body. Scale bars = 50 μm (a,e,i), 10 μm (b,b',f,f'), 20 μm (c–d,g,g'), 40 μm (h) [Color figure can be viewed at wileyonlinelibrary.com]

bleb-like and, except for one contralateral slice (Figure 15c, arrow), cover all slices of the CBU. Additional bleb-like arborizations occur within the ALI (Figure 15e) and few smooth fibers run anteriorly along the brain midline (Figure 15a, asterisk).

Two types of TU neuron with cell bodies in the posterior PI were labeled: $TU_{PI}1$ (n = 8 $TU_{PI}1$ neurons in one preparation) (Figure 16), and $TU_{PI}2$ (n = 1) (Figure 17). Somata of $TU_{PI}1$ neurons cluster in the medial PI (Figure 16a, blue circles, Figure 16b), whereas the cell body of the $TU_{PI}2$ neuron is located in the lateral PI (Figure 17a). Primary neurites of both types of neuron bend ventrally around the PB and follow the surface of the CBU toward its anterior boundary. Here, they branch and send fibers into the ipsilateral superior

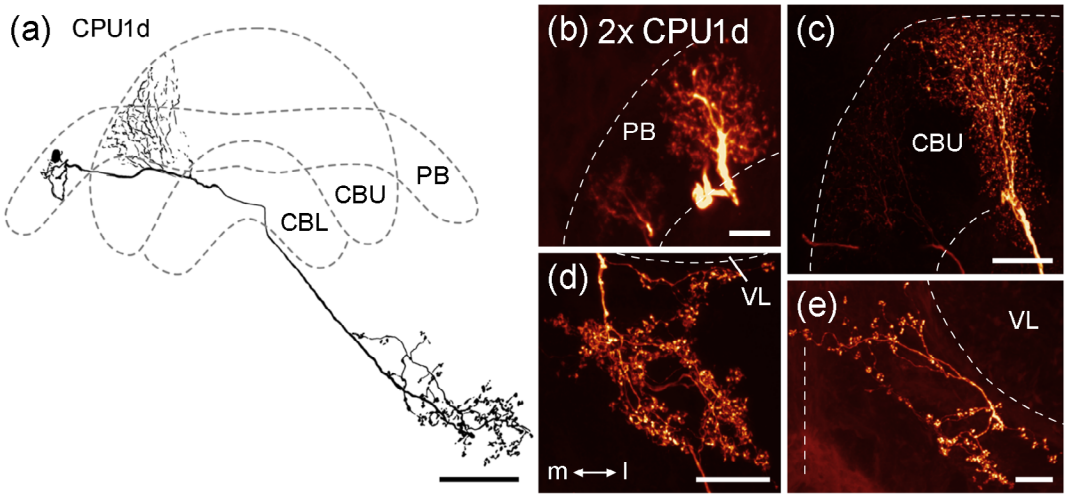

FIGURE 10 Columnar neurons of the protocerebral bridge (PB) and the upper division of the central body (CBU) with arborizations in the contralateral medial protocerebrum. (a) Reconstruction of a CPU1d neuron. (b–e) Maximum intensity visualization of arborizations of two CPU1d neurons in the PB (b), the CBU (c) and the LX (d,e). Ramifications in each neuropil are dominated by beaded specializations. Arborizations in the PB cover the width of one slice. In the CBU, arborizations cover the width of one slice in ventral regions and the width of at least two slices in dorsal regions. Bleb-like terminals cover an area ventral and medial to the vertical lobe (VL) of the mushroom body. Few terminals cross the brain midline (indicated by the vertical dashed line in (e)). CBL, lower division of the central body; m, medial; l, lateral. Scale bars = 50 μm (a), 10 μm (b), 20 μm (c–e) [Color figure can be viewed at wileyonlinelibrary.com]

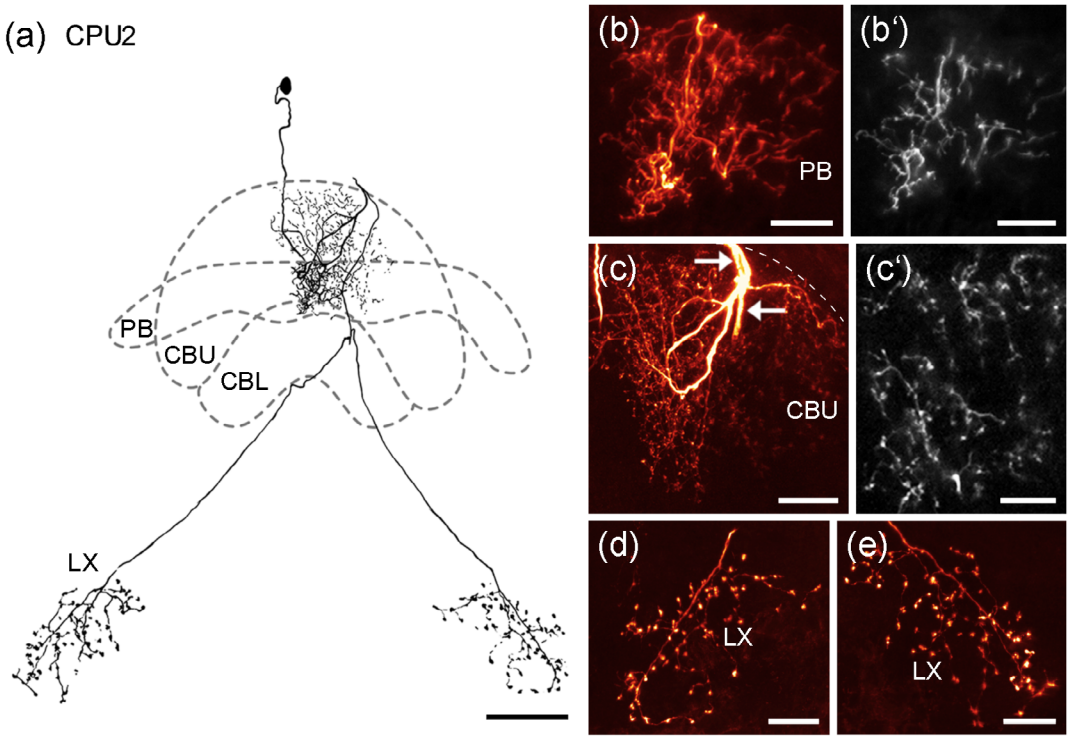

FIGURE 11 Columnar neuron of the protocerebral bridge (PB), the upper division of the central body (CBU) and both lateral complexes (LX). (a) Reconstruction of a CPU2 neuron. (b–e) Maximum intensity visualization of arborization trees of the CPU2 neuron shown in (a) in the PB (b), the CBU (c) and both LX (d,e) and of five (b′) resp. ten (c′) optical slices depicting arborizations in the PB and CBU, respectively. Arborizations in the PB are smooth, whereas bleb-like specializations dominate the CBU. Prominent bleb-like endings are formed in both LX. Arrows in (c) point to the neurite of another neuron, which bypasses the CBU. CBL, lower division of the central body. Scale bars = 50 μm (a), 10 μm (b,b′,c′), 20 μm (c,d,e) [Color figure can be viewed at wileyonlinelibrary.com]

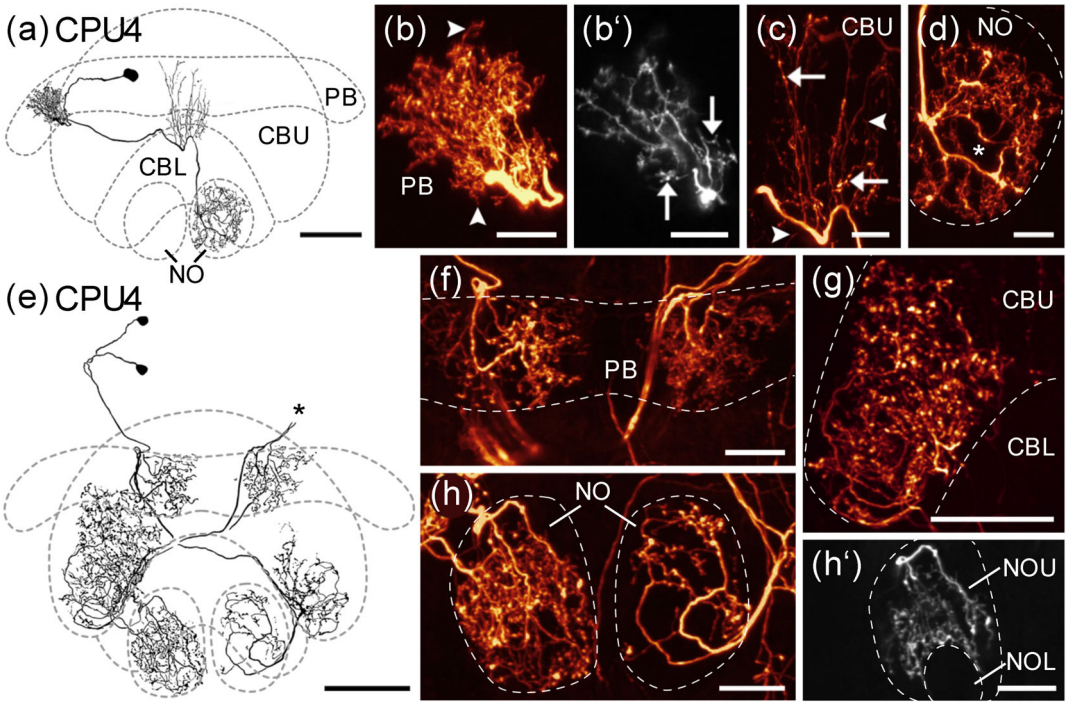

FIGURE 12 Columnar neurons of the protocerebral bridge (PB), the upper division of the central body (CBU) and the noduli (NO). (a) Reconstruction of a single CPU4 neuron. (b–d) Maximum intensity visualization of arborization trees of the CPU4 neuron shown in (a) in the PB (b), the CBU (c) and the contralateral nodulus (d), and of five optical slices depicting the PB arborizations (b′). (b,b′) Ramifications in the PB have bleb-like (arrows) as well as smooth (arrowheads) specializations. (c) Sparse processes with bleb-like structures (arrows) terminate within the CBU. Some arborizations belong to another type of neuron, that was also stained (arrowheads). (d) The CPU4 neuron possesses mixed terminals in the contralateral nodulus. It does not arborize in the lower unit of the nodulus (asterisk) and does not innervate the whole upper unit of the nodulus. (e) Reconstruction of five CPU4 neurons in one preparation. The soma location was not identifiable for some of the neurons (asterisk). They innervate medial slices of the PB and outer slices of the CBU. (f–h) Maximum intensity visualization of arborization trees of all five neurons in the PB (f) and the NO (h) and of three neurons in the CBU (g). Ramifications in all three neuropils appear predominantly varicose. (h′) Maximum intensity visualization of five optical slices depicting arborizations in the left nodulus. Arborizations in the upper unit of the nodulus (NOU) are restricted to distinct regions, as some parts are free from ramifications. The lower unit of the nodulus (NOL) is not innervated. CBL, lower division of the central body. Scale bars = 40 μm (a,g), 10 μm (b–d), 50 μm (e), 20 μm (f,h,h′) [Color figure can be viewed at wileyonlinelibrary.com]

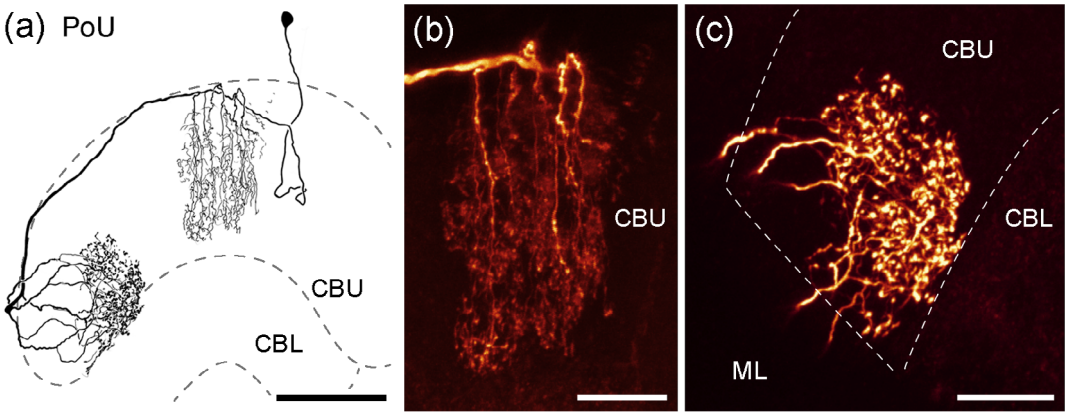

FIGURE 13 Pontine neuron with two arborization areas in the upper division of the central body (CBU). (a) Reconstruction of a PoU neuron. (b,c) Maximum intensity visualization of arborization trees in medial slices (b) and the contralateral outermost slice (c) of the CBU. Medial slices are occupied by fine processes with mixed specializations, whereas terminals in the outermost slice appear bleb-like. CBL, lower division of the central body; ML, medial lobe of the mushroom body. Scale bars = 50 μm (a), 20 μm (b,c) [Color figure can be viewed at wileyonlinelibrary.com]

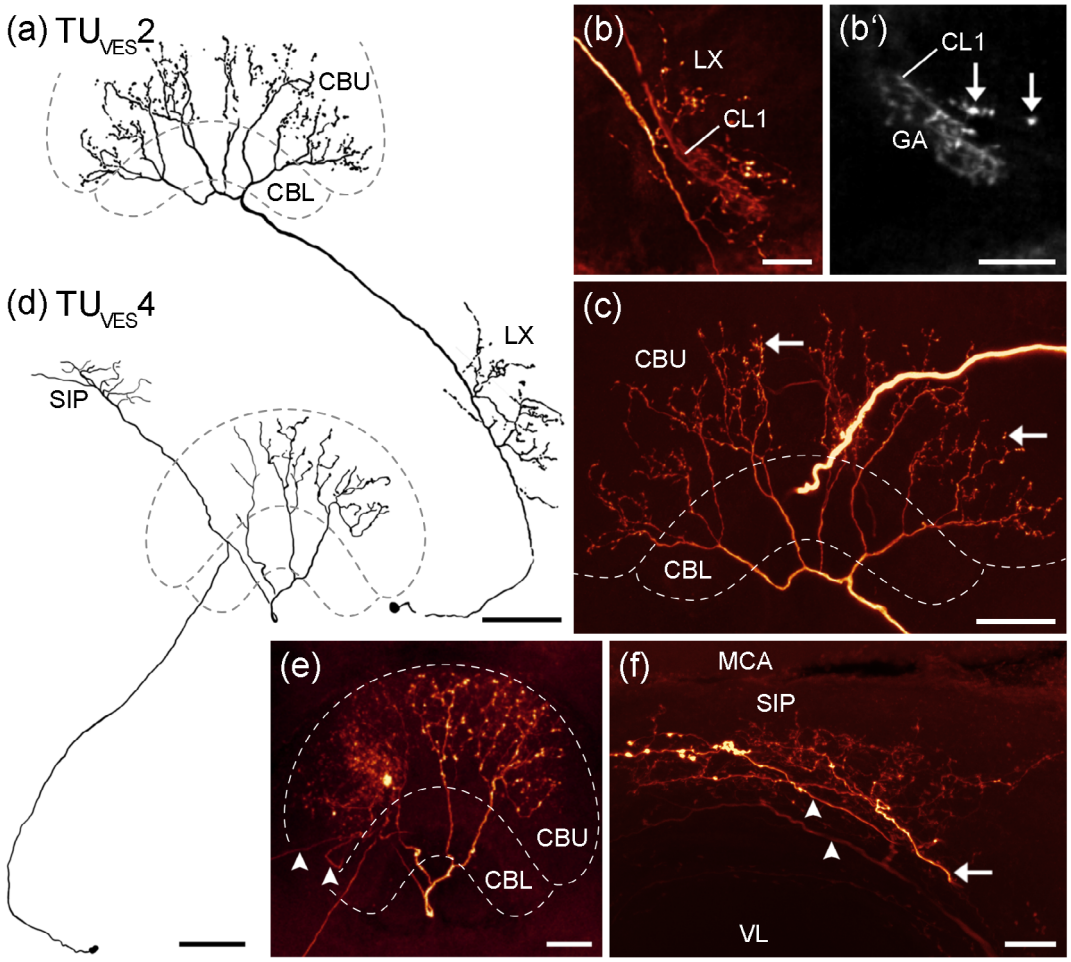

FIGURE 14 Tangential neurons of the upper division of the central body (CBU) with somata medial to the antennal lobe. (a) Reconstruction of a $TU_{VES}2$ neuron with arborizations in the CBU and the lateral complex (LX). (b,c) Maximum intensity visualization of varicose branches of the $TU_{VES}2$ shown in (a) in the LX (b) and the CBU (c) and of 10 optical slices depicting arborizations of a colabeled CL1 neuron in the gall (GA) (b′). Ramifications in the LX are predominantly bleb-like and are located mainly posteriorly to the GA. Only few terminals of the $TU_{VES}2$ neuron extend into more anterior regions (b′, arrows). Bleb-like specializations can also be found in the CBU (c, arrows). (d) Reconstruction of a $TU_{VES}4$ neuron with arborizations in the CBU and the superior intermediate protocerebrum (SIP). Due to staining of additional neurons, processes in the left hemisphere of the CBU could not be traced completely. The neuron innervates the most anterior region of the CBU but omits lateral domains of the CBU. (e,f) Maximum intensity visualization of ramifications of the $TU_{VES}4$ neuron shown in (d) in the CBU (e) and the SIP (f). Arrowheads point to neurites of other types of neuron. Ramifications in the CBU exhibit bleb-like structures. (f) Branches of the $TU_{VES}4$ neuron (arrow) cannot be distinguished from those of additionally labeled cells (arrowheads). CBL, lower division of the central body; MCA, medial calyx; VL, vertical lobe of the mushroom body. Scale bars = 50 μm (a,d), 20 μm (b,b′), 30 μm (c–f) [Color figure can be viewed at wileyonlinelibrary.com]

protocerebrum and the CBU. Whereas $TU_{PI}1$ neurons exhibit additional arborizations antero-ventral to the SMP (Figure 16b,c, arrows) the $TU_{PI}2$ neuron possesses arborizations with bleb-like endings in the ALI (Figure 17b). $TU_{PI}1$ neurons have mixed terminals within the SMP and SIP (Figure 16c). Arborizations of the $TU_{PI}2$ neuron in the SMP and SIP appear smooth (Figure 17d). Within the CBU ramification of both, $TU_{PI}1$ and $TU_{PI}2$ neurons, are dominated by the appearance of bleb-like structures (Figures 16d,e and 17c). $TU_{PI}1$ neurons sparsely innervate the anterior CBU (Figure 16d) and arborize dorsally within the medial CBU (Figure 16e). Arborizations of $TU_{PI}2$ neurons are restricted to the anterior CBU. Since eight $TU_{PI}1$ neurons were stained in the same preparation, we were not able to determine the exact innervation pattern of each individual neuron. The $TU_{PI}2$ neuron was labeled together with at least two pontine neurons (PoU, Figure 17a) that innervate two slices of the CBU (Figure 17c, arrows).

TU neurons of a third group ($TU_{SLP}1$–$TU_{SLP}4$) have their somata near the SLP along the ventral boundary of the lateral calyx of the mushroom body (LCA). The $TU_{SLP}1$ neuron (n = 1) and $TU_{SLP}2$ neurons (n = 2) (Figure 18) have arborizations in the superior protocerebrum and the CBU. The $TU_{SLP}3$ (n = 1) and $TU_{SLP}4$ neuron (n = 1) (Figure 19) additionally arborize medial to the VL. The neurons project via the anterior bundles to the central body and enter the CBU either along its anterior face ($TU_{SLP}1$, $TU_{SLP}3$, and $TU_{SLP}4$) or, after bypassing the CBL antero-ventrally, from the ventral groove ($TU_{SLP}2$).

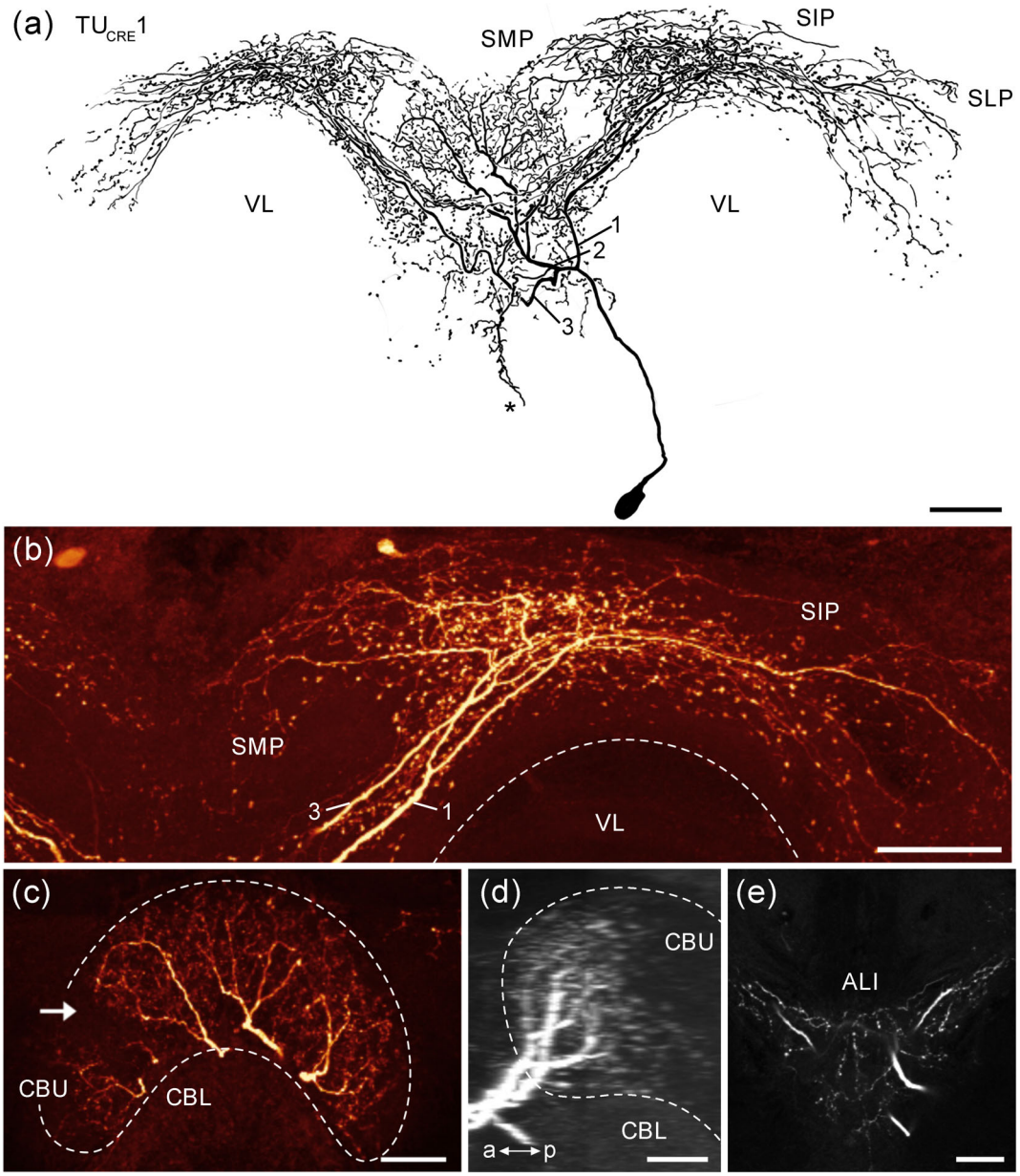

FIGURE 15 Tangential neuron of the CBU with soma anterior-medial to the antennal lobe. (a) Reconstruction of a TU$_{CRE}$1 neuron. The neuron arborizes in the superior protocerebrum of both hemispheres, the anterior lip (ALI) and the CBU. Single processes run anterior along the midline of the brain (asterisk). (b,c) Maximum intensity visualization of arborizations in the superior protocerebrum of the ipsilateral hemisphere (b), and the CBU (c). Three thick side branches are labeled (1–3 in (a); 1,3 in (b)). Branch 1 projects into the ipsilateral superior protocerebrum. Branch 2 gives rise to arborizations in the CBU and Branch 3 projects into the ipsi- and contralateral superior protocerebrum. (c) One region within the CBU appears to lack staining (arrow). (d) Sagittal view of a maximum intensity visualization of arborizations within the CBU. (e) Maximum intensity visualization of five optical slices depicting branches of the neuron in the ALI. A, anterior; CBL, lower division of the central body; VL, vertical lobe of the mushroom body; p, posterior. Scale bars = 50 μm (a,b), 25 μm (d), 30 μm (c,e) [Color figure can be viewed at wileyonlinelibrary.com]

The soma of the TU$_{SLP}$1 neuron is located ventral to the medial portion of the LCA (Figure 18a), whereas TU$_{SLP}$2 neurons have their somata at its ventro-lateral edge (Figure 18b). Both types of neuron project medially and innervate the SIP (TU$_{SLP}$1) or the SIP and SMP (TU$_{SLP}$2). Ramifications of the TU$_{SLP}$1 neuron within the SIP have a predominantly bleb-like appearance (Figure 18c). The innervation pattern of the neuron within the CBU was not characterized in detail, because additional neurons were stained in this area. Arborizations of the TU$_{SLP}$2 neuron within the SIP and SMP appear fine with bleb-like structures (Figure 18d). Ramifications within the CBU are restricted to posterior regions of all slices and possess prominent bleb-like endings (Figure 18e).

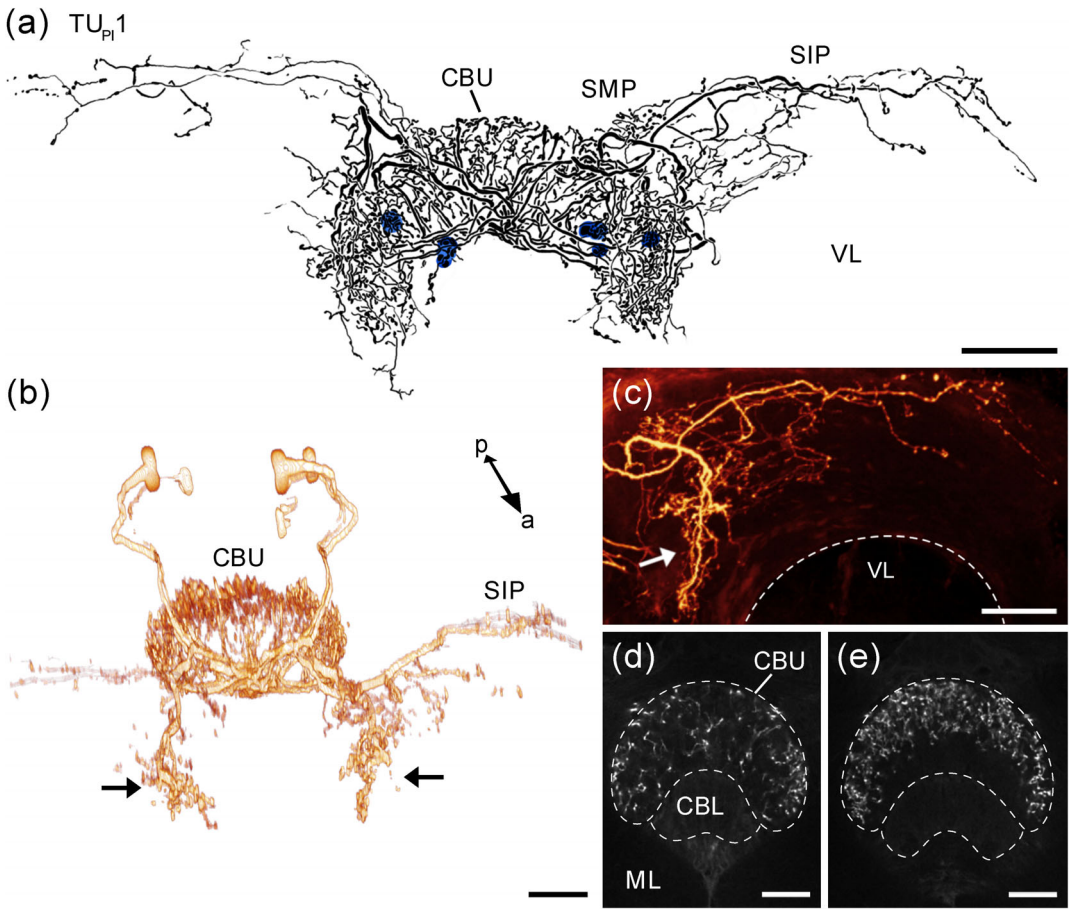

FIGURE 16 Tangential neurons of the CBU with cell bodies in the pars intercerebralis. (a) Reconstruction of a group of $TU_{PI}1$ neurons. Eight cell bodies (blue filled circles) are located posterior to the innervated regions. (b) 3D volume rendering of the staining. (c) Maximum intensity visualization of arborizations in the superior protocerebrum. (d) Optical slice depicting arborizations in the anterior CBU. (e) Optical slice depicting arborizations in the medial CBU. The $TU_{PI}1$ neuron ramifies in the superior medial protocerebrum (SMP), the superior intermediate protocerebrum (SIP), antero-ventral to the SMP (arrows in (b,c)) and in the CBU. Arborizations within the CBU cover the anterior CBU and dorsal regions of the medial CBU. A, anterior; CBL, lower division of the central body; ML, medial lobe of the mushroom body; VL, vertical lobe of the mushroom body; p, posterior. Scale bars = 50 μm (a), 40 μm (b), 20 μm (c), 40 μm (d,e) [Color figure can be viewed at wileyonlinelibrary.com]

The $TU_{SLP}3$ neuron (Figure 19a–c) has its soma ventral to the medial portion of the LCA (Figure 19a). The primary neurite projects medially and gives off side branches into the SMP (Figure 19a,b). Noticeably, some fibers proceed further anterior and arborize medially along the VL (Figure 19a, arrow). Due to the labeling of additional TU neurons in the same preparation (Figure 19c, arrows), we were not able to determine the detailed innervation pattern of the $TU_{SLP}3$ neuron (Figure 19c, arrowhead) within the CBU.

The soma of the $TU_{SLP}4$ neuron (Figure 19d,e) is located at the ventro-lateral edge of the LCA (Figure 19d). The primary neurite projects medially toward the brain midline. Several side branches originate from the primary neurite and innervate the ipsilateral SMP and regions medial to the VL. Some processes also extend into the contralateral hemisphere. Anterior to the CBL the main neurite turns dorsally and splits into several branches. They run along the dorsal surface of the CBU, sending processes into all slices. The structure of terminals within the CBU appears bleb-like (Figure 19e). The most anterior region of each slice is not innervated.

3.7 | Tangential neurons of the NO

We identified two neurons with ramifications in the NO (TN1, n = 1 and TN2, n = 1, Figure 20). Cell bodies of both neurons are located medially to the AL, similar to those of TL1 neurons and the $TU_{CRE}1$ neuron, and their neurites take the same path, that is, they project posteriorly around the AL and dorso-medially through the LX. The TN1 neuron innervates the LX (Figure 20a). Due to staining of additional neurons in the same preparation (data not shown), we could not reconstruct all its ramifications in this area. In contrast, the TN2 neuron has most ramifications in the lateral protocerebrum and sends only few fine processes into the LX (Figure 20c). Both types of neuron

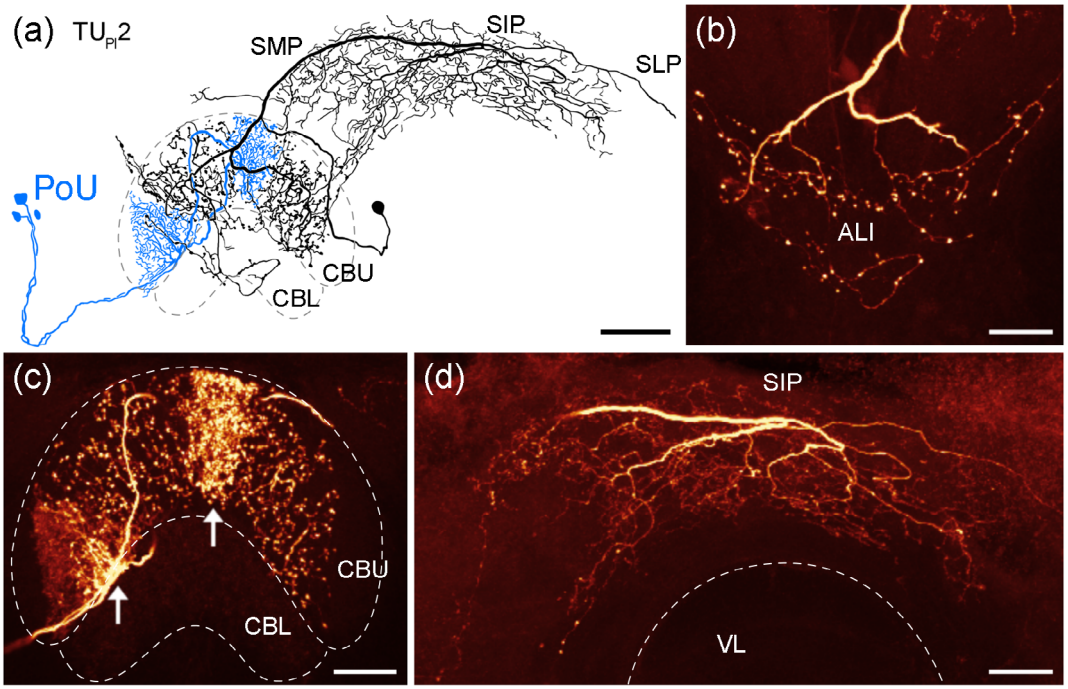

FIGURE 17 Tangential neuron of the CBU with cell body in the pars intercerebralis. (a) Reconstruction of a TU$_{PI}$2 neuron (black) and few pontine neurons (PoU) (blue). (b–d) Maximum intensity visualization of arborizations in the anterior lip (ALI), the CBU, and the superior protocerebrum, respectively. (b,c) Ramifications of the TU$_{PI}$2 neuron in the ALI and the CBU have bleb-like specializations. Arrows in (c) indicate arborization areas of the PoU neurons. (d) Ramifications in the superior protocerebrum are concentrated in the superior intermediate protocerebrum (SIP) and appear smooth. CBL, lower division of the central body; SLP, superior lateral protocerebrum; SMP, superior medial protocerebrum; VL, vertical lobe of the mushroom body. Scale bars = 50 μm (a), 30 μm (b–d) [Color figure can be viewed at wileyonlinelibrary.com]

have bleb-like endings in the ipsilateral NOU but do not innervate the NOL (Figure 20b,b′,d,d′).

4 | DISCUSSION

Using iontophoretic dye injections we characterized 17 types of CX neuron (Figure 21, Table 1). Some of them comprise several subtypes, resulting in a total of 24 morphologically distinct types of neuron. Most of them can be related to neuronal cell types described in other insect species. A table of presumably homologous types of neuron and respective names in *D. melanogaster* and other insect species has been published by Franconville, Beron, and Jayaraman (2018) and Honkanen et al. (2019). In the following paragraphs, we will discuss morphological similarities and differences between CX neurons in the honeybee and other insect species as well as possible functions.

4.1 | Sample size

Our sample size varied for different types of neuron. It is lowest with $n = 1$ for most types of TU neuron and relatively high with $n = 19$ for CL1 neurons. Nevertheless, we consider features, like cell body position, trajectory of the primary neurite, or the region where the neuron enters the CBU, as reliable for classification, as they turned out to be consistent in neuronal cell types that were stained in multiple preparations. Furthermore, these features are even largely consistent not only between individuals, but across species borders. For example, the classification of two different subtypes of CPU1a neuron is supported by the description of two CPU1a subtypes in monarch butterflies and bogong moths (*Agrotis infusa*) (de Vries et al., 2017; Heinze et al., 2013). The same holds true for differentiating between TN1 and TN2 neurons (with $n = 1$ for each), which have been classified on basis of larger sample size in the sweat bee (Stone et al., 2017) and have also been identified in the locust (von Hadeln et al., 2020). Especially in cases, where other types of neuron were colabeled together with TU neurons, however, detailed morphology still needs to be determined.

4.2 | Neuron polarity

Since function is related to the polarity of neurons, we pointed to morphological features of arborization areas, that is, whether they are smooth/fine or varicose/bleb-like, indicating input or output sites, respectively. An electron microscopical study in *Drosophila* has shown that the shape of neuronal branches is a good predictor for input/output regions (Cardona et al., 2010). Nevertheless, this type of analysis

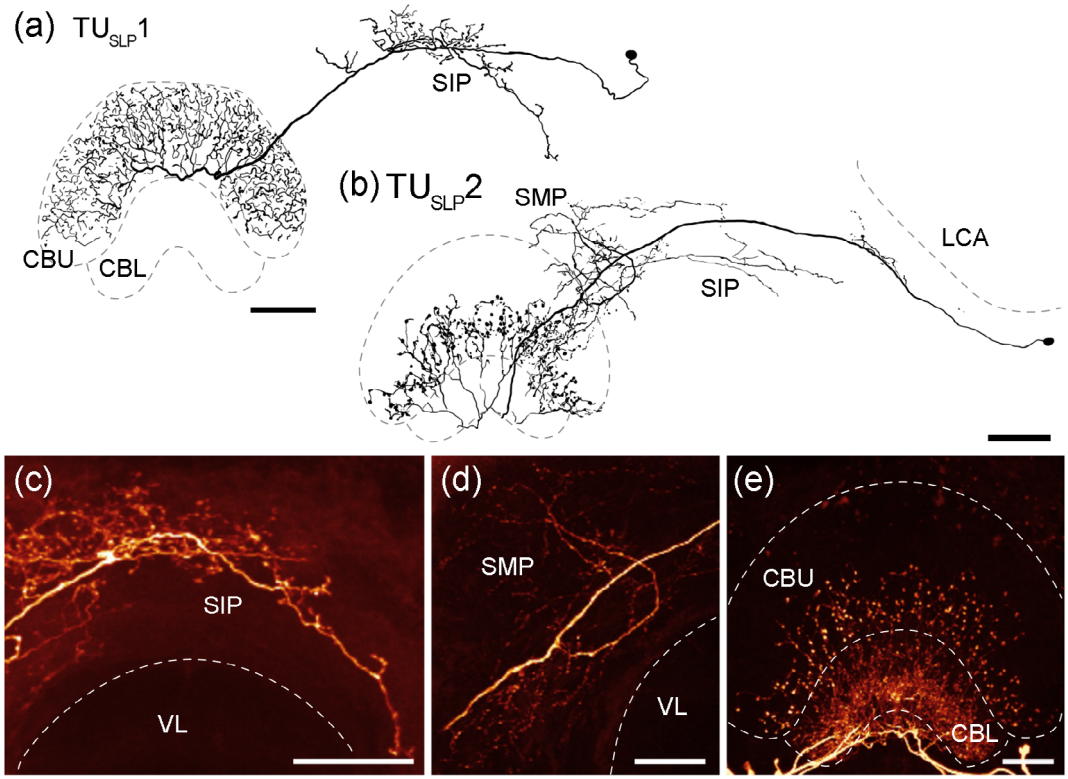

FIGURE 18 Tangential neurons of the CBU with cell bodies ventral to the lateral calyx (LCA). (a) Reconstruction of a $TU_{SLP}1$ neuron. The cell body of this neuron is located at the medial boundary of the LCA. The neuron arborizes in the superior intermediate protocerebrum (SIP) and the CBU. (b) Reconstruction of a $TU_{SLP}2$ neuron. The cell body is located at the lateral boundary of the LCA. The neuron arborizes in the SIP, the superior medial protocerebrum (SMP) and the CBU. (c) Maximum intensity visualization of arborizations of the $TU_{SLP}1$ neuron shown in (a) in the SIP. (d,e) Maximum intensity visualization of arborizations of the $TU_{SLP}2$ neuron shown in (b) in the SMP and the CBU, respectively. (e) Several types of tangential neuron that innervate the lower division of the central body (CBL) were stained in the same preparation. VL, vertical lobe of the mushroom body. Scale bars = 50 μm (a,b,c), 30 μm (d,e) [Color figure can be viewed at wileyonlinelibrary.com]

has to be interpreted cautiously, as unambiguous identification of input and output areas has to be done on EM-level or by performing physiological experiments. Varicose or smooth appearance was predominant in many areas, whereas some arborization areas exhibited mixed features (Figure 21). Moreover, morphological features could not be determined in some cases, or need to be reevaluated when additional samples are available (e.g. in case of $TU_{VES}2$, CPU1d). Dendrites of TL2 and TL3 neurons have been investigated already in more detail (locust: Träger et al., 2008; honeybee: Held et al., 2016), since they form conspicuous structures, termed microglomerular synaptic complexes, with their presynaptic partners in the LBU and MBU of the LX.

4.3 | Neurons of the core compass network

From work on a number of insect species, a ground pattern of the core compass network, which generates and maintains a neuronal representation of the animal's heading with respect to external cues, has emerged. This network comprises an input stage (TL, TN or ring [R] neurons, NO neurons in *Drosophila*), an intermediate stage (CL1, CL2, TB or E-PG, P-EN, Δ7 neurons) and an output stage (CPU1, CPU2, or PFI neurons). We were able to stain all cell types of the core compass network, except for TB neurons.

TL2 and TL3 might constitute the most prominent elements of the input stage. They have been described as polarization-sensitive in the desert locust *Schistocerca gregaria* (e.g. Pegel et al., 2018; Vitzthum et al., 2002), the monarch butterfly *Danaus plexippus* (Heinze & Reppert, 2011), the dung beetles *Scarabeus lamarckii* and *Scarabeus satyrus* (el Jundi et al., 2015) and the tropical nocturnal sweat bee *M. genalis* (Stone et al., 2017). TL2 and TL3 neurons receive input from two different types of neuron of the anterior optic tubercle via specialized microglomerular synaptic complexes, in the LBU and MBU, respectively (Held et al., 2016; Träger et al., 2008). As a consequence, they transmit visual information via two parallel pathways toward the CX. In contrast to locusts and honeybees, fruit flies and monarch butterflies possess a single BU, without spatially separated subcompartments. Nevertheless, segregated parallel pathways into the CBL (EB) via TL-like neurons (ring neurons) also exist (Heinze et al., 2013; Omoto et al., 2017; Shiozaki & Kazama, 2017). Moreover, specific connectivity patterns between the LBU or MBU (BU partitions) and CBL layers (EB annular domains) have been shown for the fruit fly (Omoto et al., 2017; Omoto et al., 2018), the locust (Müller et al., 1997; Pegel, Pfeiffer, Zittrell, Scholtyssek, &

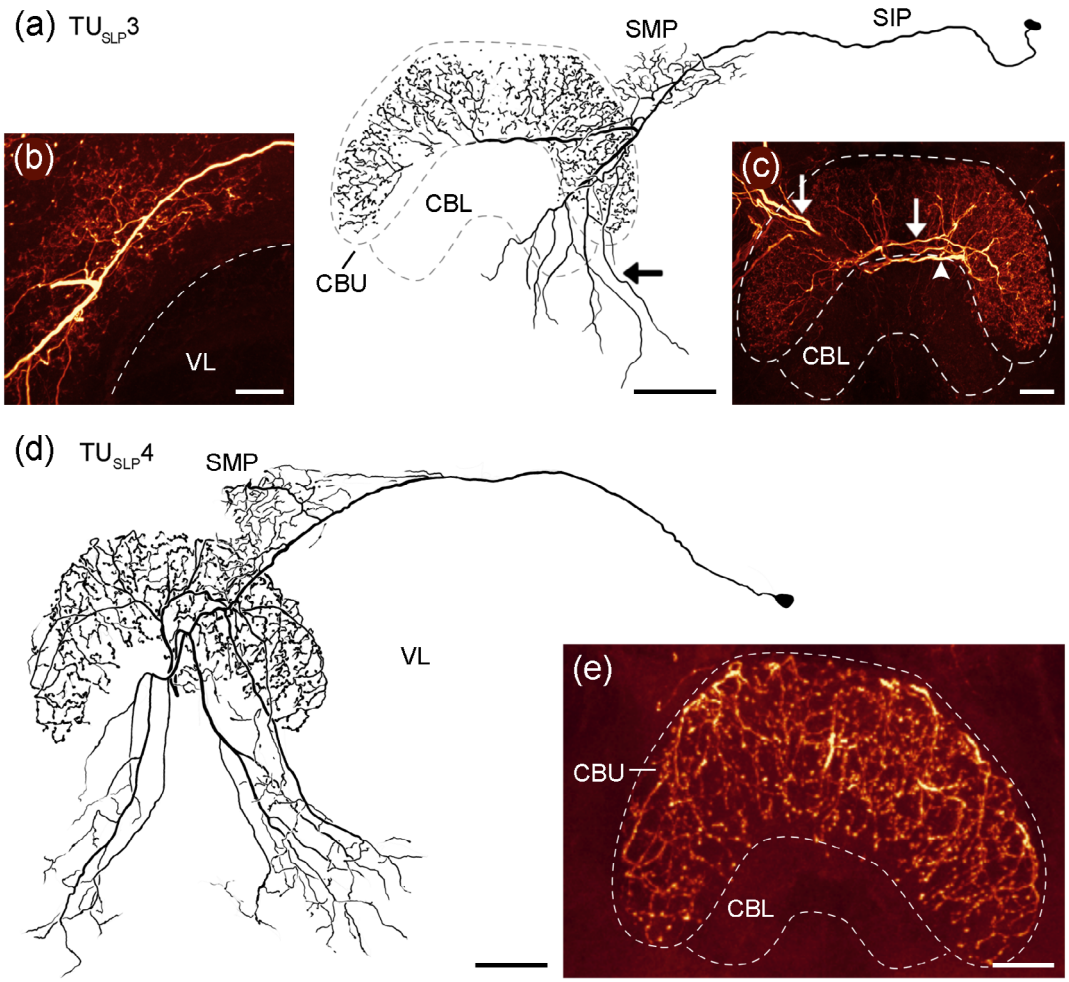

FIGURE 19 Tangential neurons of the CBU with cell bodies ventral to the lateral calyx (LCA). (a) Reconstruction of a $TU_{SLP}3$ neuron. The neuron innervates the superior medial protocerebrum (SMP) and a region medial to the vertical lobe (VL) of the mushroom body (arrow). (b,c) Maximum intensity visualization of arborizations in the SMP and the CBU, respectively. The arrowhead in (c) points to the $TU_{SLP}3$ neuron. Arrows indicate processes of additionally stained neurons. (d) Reconstruction of a $TU_{SLP}4$ neuron. The neuron arborizes in the ipsilateral SMP and medial to the VL of both hemispheres. (e) Maximum intensity visualization of varicose arborizations of the $TU_{SLP}4$ neuron in the CBU. CBL, lower division of the central body; VL, vertical lobe of the mushroom body. Scale bars = 50 μm (a,d), 20 μm (b,c), 30 μm (e) [Color figure can be viewed at wileyonlinelibrary.com]

Homberg, 2019; von Hadeln et al., 2020) and the monarch butterfly (Heinze et al., 2013). In accordance with these findings, TL2 and TL3 neurons in the honeybee target distinct regions within the CBL. Specifically, we could distinguish between a ventral layer of the CBL, which extends from anterior to posterior and houses ramifications of TL2 neurons, and the space in between that is occupied by arborizations of TL3 neurons. TL1 and TL6 neurons appear to innervate similar regions as TL3 neurons. However, the high number of layers (annular domains) in the other insect species (six in locusts, four in monarch butterflies, and five in fruit flies) suggests that more types/subtypes of TL neuron exist in the honeybee than have been described in this account. The same holds true for the BUs, which appear to be further compartmentalized by arborizations of TL2 subtypes in locusts and monarch butterflies and R3 subtypes as well as R2, R4, and R5 neurons in the fruit fly. Beyond the role in compass orientation, more recent evidence shows a function of neurons branching in the bulbs in sleep control (Donlea et al., 2018; Liu et al., 2006). This seems to be mediated by direct input from so called anteriorly projecting dorsal neurons of the circadian network to neurons of the anterior optic tubercle, which in turn drive ring neurons (Guo, Holla, Díaz, & Rosbash, 2018; Lamaze, Krätschmer, Chen, Lowe, & Jepson, 2018). While this circadian input has so far only been shown to play a role in sleep and wakefulness, it could also deliver the signals that are necessary for the time compensation of sky-compass signals.

Like TL2 and TL3 neurons, TL1 neurons play a role in processing visual information. In locusts, they are sensitive to different visual cues including polarized light (Pegel et al., 2018; Vitzthum et al., 2002). One TL1 neuron recorded in the honeybee responded to moving visual stimuli (Homberg, 1985). In that report, polarized light was not used as a stimulus. In contrast to TL2 and TL3 neurons, TL1 neurons arborize within the LAL and the GA instead of the BU. Amongst TL-like neurons (R neurons and ExR neurons) in

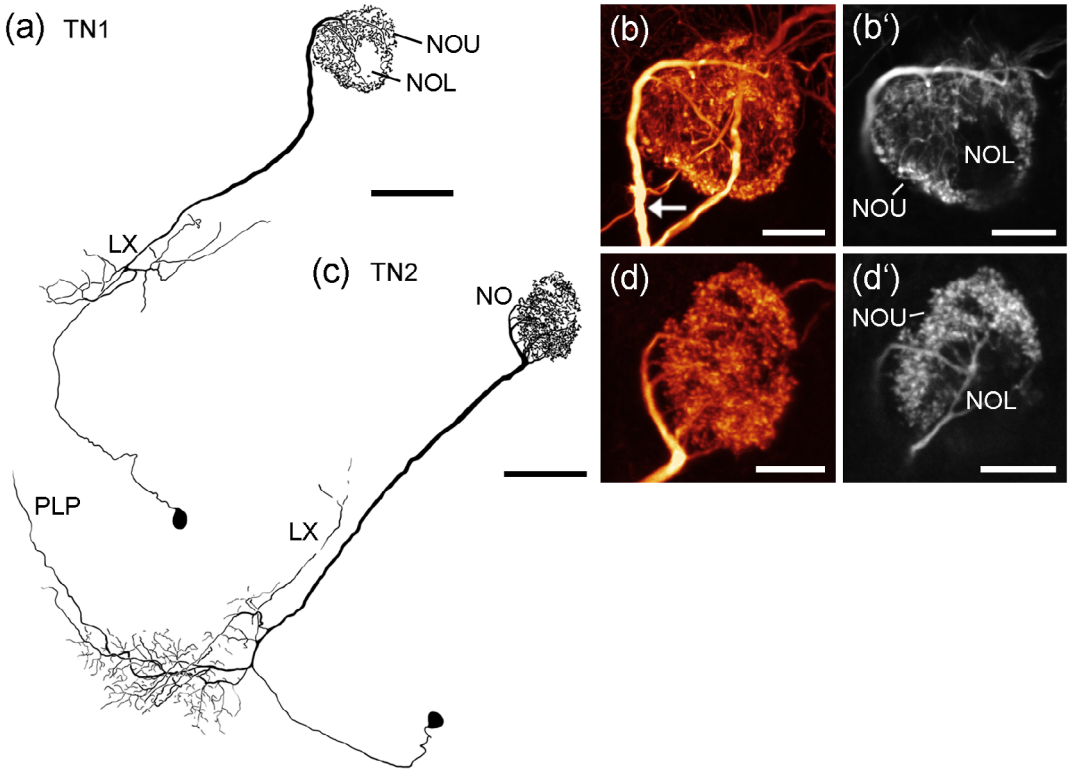

FIGURE 20 Tangential neurons of the noduli (NO) with arborizations in the ventral protocerebrum. (a) Reconstruction of a TN1 neuron. The neuron arborizes within the lateral complex (LX) and the ipsilateral nodulus. Note that not all arborizations within the LX were reconstructed, as additional neurons were stained in this area. (b,b′) Maximum intensity visualization of the whole arborization tree of the TN1 neuron in the ipsilateral nodulus (b) and of five optical slices (b′). Large areas of the upper unit of the nodulus (NOU) are innervated by bleb-like terminals of the TN1 neuron (arrow). (b′) The lower unit of the nodulus (NOL) is not innervated. (c) Reconstruction of a TN2 neuron. The neuron arborizes in the LX and the posterior lateral protocerebrum (PLP). (d,d′) Maximum intensity visualization of the whole arborization tree of the TN2 neuron in the ipsilateral nodulus (d) and of five optical slices (d′). The TN2 neuron has bleb-like specializations within the NOU. The NOL is free from ramifications. Scale bars = 50 μm (a,c), 20 μm (b,b′,d,d′) [Color figure can be viewed at wileyonlinelibrary.com]

Drosophila some show similar arborization patterns (Franconville et al., 2018; Omoto et al., 2018) and TL1 neurons of the monarch butterfly have also been reported to innervate the GA (anterior loblet, Heinze et al., 2013).

At the intermediate stage of the core compass network, CL1 neurons transmit information between the CBL, PB, and the GA. Coding of visual cues has been described for CL1 neurons in locusts (Heinze & Homberg, 2009; Pegel et al., 2018; Rosner & Homberg, 2013), monarch butterflies (Heinze & Reppert, 2011), dung beetles (el Jundi et al., 2015), sweat bees (Stone et al., 2017), and fruit flies (Seelig & Jayaraman, 2013). In the honeybee, CL1 neurons respond to simultaneous stimulation with illumination and wind (Milde, 1988) or light and wind stimuli alone (Homberg, 1985). Differences in the dendrite-axon polarity and in the area of arborization within the CBL characterize different subtypes of CL1 neuron (CL1a–CL1d, Heinze & Homberg, 2008). Due to their polarity CL1a (E-PG) neurons are most likely candidates to forward information from the CBL to the PB, whereas CL1b (P-EG) neurons might signal in the opposite direction (Heinze et al., 2013; Heinze & Homberg, 2008). Terminals of most CL1 neurons described here appear mixed in the PB and the CBL. We are therefore not able to infer their polarity and to assign them to any of the CL1 subtypes described in other insects. Nevertheless, one CL1 neuron differed from the others in morphological structure of its terminals and might, therefore, represent a different CL1 subtype.

In *Drosophila*, CL1a (E-PG) and CL2 (P-EN) neurons establish a network that keeps track of angular heading (Green et al., 2017; Turner-Evans et al., 2017). In locusts, CL2 neurons are polarization-sensitive (Heinze & Homberg, 2009) and respond to stimuli simulating rotation around the yaw axis (Pegel, 2018). Morphologically CL2 neurons were also described in the monarch butterfly, the dung beetle and the bumblebee (*Bombus terrestris*; el Jundi et al., 2018; Heinze et al., 2013; Stone et al., 2017). Polarity of CL2 neurons of the honeybee as well as the different interhemispheric wiring schemes of CL1 and CL2 neurons meet the conditions requested by the network model for angular integration (Green et al., 2017; Turner-Evans et al., 2017), that is, CL1 and CL2 neurons arborizing in the same slice of the PB innervate neighboring slices within the CBL (data not shown).

Major output of the CX network toward premotor centers is presumably provided by CPU1 and CPU2 neurons (PFI neurons in

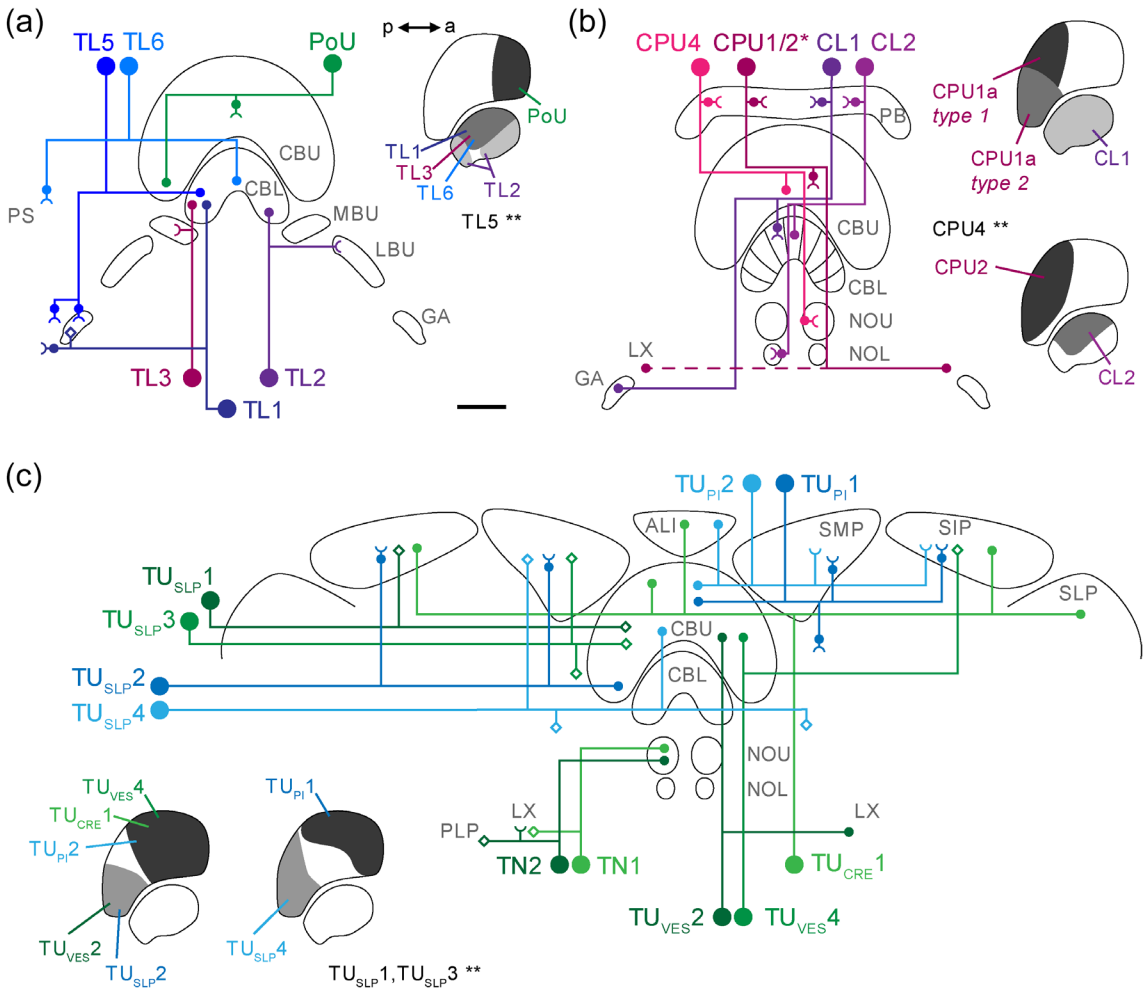

FIGURE 21 Schematic illustration of branching patterns and approximate branching areas of neurons that arborize in the central complex. (a) Tangential neurons of the lower division of the central body (CBL; TL neurons) and a pontine neuron of the upper division of the central body (CBU; PoU neuron). (b) Columnar neurons of the CBL (CL neurons) and the CBU (CPU neurons). (c) Tangential neurons of the CBU (TU neurons). Cell bodies are indicated by large, filled circles. Small, filled circles indicate presumed output, whereas semicircles indicate presumed input. Open rhombs indicate undefined terminals. Schematic sagittal views in (a–c) depict innervated areas within the CBU and CBL. * in (b): For sake of clarity, CPU1a *Type 1* and *2* and CPU1d and CPU2 neurons are not depicted individually. Only CPU2 neurons innervate the lateral complex (LX) of both hemispheres, therefore an additional neurite is depicted with a dashed line. ** in (a–c): Innervation pattern of these neurons within the CBL or CBU could not be determined due to faint staining or additionally labeled neurons in the respective preparation. ALI, anterior lip; GA, gall; LBU, lateral bulb; MBU, medial bulb; NOL, lower unit of the nodulus; NOU, upper unit of the nodulus; PB, protocerebral bridge; PLP, posterior lateral protocerebrum; PS, posterior slope; SIP, superior intermediate protocerebrum; SLP, superior lateral protocerebrum; SMP, superior medial protocerebrum. Scale bar = 50 μm [Color figure can be viewed at wileyonlinelibrary.com]

Drosophila, Lin et al., 2013), as they possess large, presynaptic arborizations within the LX. CPU1 and CPU2 neurons are sensitive to visual compass stimuli in locusts (Heinze & Homberg, 2007), monarch butterflies (Heinze & Reppert, 2011), dung beetles (el Jundi et al., 2015) and the nocturnal sweat bee (Stone et al., 2017). In the honeybee, CPU1 neurons responded to different stimuli, including illumination and mechanical stimuli (Homberg, 1985). Morphologically, CPU1 neurons constitute several subtypes that exhibit differences in the extent of their arborizations and their interhemispheric wiring schemes (Heinze et al., 2013; Heinze & Homberg, 2008; Lin et al., 2013). Based on their arborizations within the CBU and the LX, two subtypes of CPU1a neuron, namely, *Type 1* and *Type 2*, were defined in *D. plexippus* (Heinze et al., 2013) and *A. infusa* (de Vries et al., 2017). Because differences in LX arborizations were most striking in the CPU1a neurons found here, we classified these types of neuron accordingly: ramifications of CPU1a *Type 2* neurons extend further ventrally and posteriorly within the LX than those of CPU1a *Type 1* neurons. In *D. melanogaster* CPU1 neuron homologues target the round body (ROB) or the LAL and crepine (CRE) in addition to the CX and are termed P-F-R or PF-LC neurons, respectively (Wolff & Rubin, 2018). They have been suggested to be homologues to CPU1a *Type 1* (PF-LC) neurons and CPU1a *Type 2* (P-F-R) neurons (Honkanen et al., 2019). More generally, both of

these types, as well as CPU2 neurons, belong to the PFI types of neuron described by Lin et al. (2013).

Despite their differences, all CPU neurons exhibit a common polarity likely transmitting information from the PB to the LX. Whether the CPU1d neuron described here represents an exception, could not be unambiguously determined.

4.4 | Tangential neurons of the NO

Neurons projecting from the LX to the NO (TN neurons or NO neurons) have been described in *Megalopta* (Stone et al., 2017), *Drosophila* (Wolff & Rubin, 2018), and *Schistocerca* (von Hadeln et al., 2020). Comparison between TN1 and TN2 neurons in *Apis* and *Megalopta* indicate that these types of neuron are morphologically similar in both species. Whereas TN1 neurons extensively innervate the LAL, TN2 neurons predominantly ramify within ventrolateral neuropils (Stone et al., 2017). Electrophysiological studies in *Megalopta* show that these cells are sensitive to anterograde or retrograde movement of bars and gratings. As in *Schistocerca*, where TN1 and TN2 neurons innervate layer II and layer III of the NOU, respectively, NO neurons in *Drosophila* constitute different subtypes that innervate distinct subunits of the NO (Wolff & Rubin, 2018).

4.5 | Tangential neurons of the CBU

In addition to tangential neurons providing input to the CBL, we identified TU neurons with presynaptic arborizations spanning different regions of the CBU. Consistent with findings in other insects, TU neurons constitute a diverse group, connecting different regions of the protocerebrum to the CBU (e.g., el Jundi et al., 2018; Heinze et al., 2013; Homberg, Vitzthum, Müller, & Binkle, 1999; Li et al., 2009; Phillips-Portillo & Strausfeld, 2012; von Hadeln et al., 2020; Weir & Dickinson, 2015; Wendt & Homberg, 1992). In the honeybee, different types of TU neuron respond to mechanical, light, motion, or olfactory stimuli (Homberg, 1985; Milde, 1988). In locusts and flesh flies activity of individual TU neurons changes upon visual and wind stimulation (Homberg, 1994; Phillips-Portillo, 2012; Rosner & Homberg, 2013). FB neurons of the fruit fly have been shown to play a role in visual pattern memory (Li et al., 2009; Liu et al., 2006), flight-gated visual responses (Weir & Dickinson, 2015), modulation of locomotor behavior (Kahsai, Martin, & Winther, 2010) and, together with TL-like neurons, in sleep control (Donlea et al., 2018). Morphologically, fan-shaped neurons of the CBU described by Homberg (1985) show striking similarities in their soma position and arborization regions to TU_{VES}, $TU_{CRE}1$, and TU_{SLP} neurons. As indicated by their name, these types of TU neuron likely correspond, or at least show strong similarities, to those described in locusts (von Hadeln et al., 2020).

4.6 | Other neurons

TL5 neurons, although exhibiting arborizations in the LX, GA, and CBL, obviously differ from TL1 to TL3 neurons regarding the location of their soma in the PI. Polarization-insensitive TL5 neurons from *Schistocerca* (Müller et al., 1997; Vitzthum et al., 2002) and posterior extrinsic ring neurons (ExR neurons) from *Drosophila* (Omoto et al., 2018) share this characteristic (von Hadeln et al., 2020).

Whereas TU neurons constitute a diverse class, with arborizations in many regions of the protocerebrum, TL neurons form a more homogenous group, mostly exhibiting arborizations in the LX. Therefore, the TL6 neuron reported here, with extensive arborizations in the posterior protocerebrum, stood out from all remaining types of TL neuron. The TL (GA-BU-POTU) neuron described in the bogong moth (de Vries et al., 2017) and TCX neurons described in the locust (von Hadeln et al., 2020) share some morphological characteristics but arborize in many compass-related brain regions and are suggested to play a modulatory or synchronizing role. In contrast, the TL6 neuron specifically targets the CBL and might be unique for the honeybee.

CPU4 (P-FN neurons in *Drosophila*, Wolff & Rubin, 2018) neurons have not been described as part of the network encoding the animals heading. In locusts however, they have been shown to be polarization-sensitive in some preparations, but not in others (Heinze & Homberg, 2009). Based on a network model of CX circuits, CPU4 neurons were hypothesized to be the neural correlate of path integration memory (Stone et al., 2017). Subtypes of CPU4 neurons innervate different layers of the NOU in locusts (CPU4a-c; Heinze & Homberg, 2008), monarch butterflies (Heinze et al., 2013), dung beetles (el Jundi et al., 2018), and fruit flies (Lin et al., 2013; Wolff et al., 2015). Although CPU4 neurons described here also innervate distinct regions within the NOU, these regions might not correspond to different NOU layers, as all neurons labeled might belong to the same subtype, which would innervate the same layer within the NOU. To define borders within the NOU based on CPU4 innervation patterns, the different subtypes need first to be identified.

CPU5 neurons morphologically resemble CPU4 neurons but innervate other layers of the CBU (Heinze & Homberg, 2008), resulting in specified connectivity patterns between layers of the CBU and the NOU. As layers within the CBU of the honeybee have not been defined so far, we did not distinguish between CPU4 and CPU5 neurons.

Taken together, our data set shows that the neuronal network building the CX of honeybees consists both of elements that are highly conserved (core compass network) as well as elements that seem to be highly specific to honeybees (TL6, TU_{PI} neurons).

ACKNOWLEDGMENTS

We are grateful to Erich Buchner and Christian Wegener for providing anti-synapsin antibodies, Joss von Hadeln for help with Amira, Katja Tschirner for providing the 3D reconstruction of the CX, and Basil el Jundi for helpful comments on the manuscript. We thank Jutta

Seyfarth for bee keeping and Martina Kern for technical assistance. This work was supported by grants from the Deutsche Forschungsgemeinschaft (PF714/4-1 to Keram Pfeiffer and HO 950/24-1 to Uwe Homberg).

DATA AVAILABILITY STATEMENT

The data that support the findings of this study are available in the insect brain data base (insectbraindb) at https://insectbraindb.org/app/neuron/dataset/a637d6a7-1b2d-4dd7-8be3-70a4c4512c01.

ORCID

Uwe Homberg https://orcid.org/0000-0002-8229-7236
Keram Pfeiffer https://orcid.org/0000-0001-5348-2304

REFERENCES

Barron, A. B., & Plath, J. A. (2017). The evolution of honey bee dance communication: A mechanistic perspective. *Journal of Experimental Biology*, *220*, 4339–4346. https://doi.org/10.1242/jeb.142778

Bender, J. A., Pollack, A. J., & Ritzmann, R. E. (2010). Neural activity in the central complex of the insect brain is linked to locomotor changes. *Current Biology*, *20*, 921–926. https://doi.org/10.1016/j.cub.2010.03.054

Brandt, R., Rohlfing, T., Rybak, J., Krofczik, S., Maye, A., Westerhoff, M., … Menzel, R. (2005). Three-dimensional average-shape atlas of the honeybee brain and its applications. *Journal of Comparative Neurology*, *492*, 1–19. https://doi.org/10.1002/cne.20644

Buchanan, S. M., Kain, J. S., & de Bivort, B. L. (2015). Neuronal control of locomotor handedness in *Drosophila*. *Proceedings of the National Academy of Sciences of the United States of America*, *112*, 6700–6705. https://doi.org/10.1073/pnas.1500804112

Cardona, A., Saalfeld, S., Preibisch, S., Schmid, B., Cheng, A., Pulokas, J., … Hartenstein, V. (2010). An integrated micro-and macroarchitectural analysis of the *Drosophila* brain by computer-assisted serial section electron microscopy. *PLoS Biology*, *8*, e1000502. https://doi.org/10.1371/journal.pbio.1000502

de Vries, L., Pfeiffer, K., Trebels, B., Adden, A. K., Green, K., Warrant, E., & Heinze, S. (2017). Comparison of navigation-related brain regions in migratory versus non-migratory noctuid moths. *Frontiers in Behavioral Neuroscience*, *11*, 158. https://doi.org/10.3389/fnbeh.2017.00158

Dent, J. A., Polson, A. G., & Klymkowsky, M. W. (1989). A whole-mount immunocytochemical analysis of the expression of the intermediate filament protein vimentin in *Xenopus*. *Development*, *105*, 61–74.

Donlea, J. M., Pimentel, D., Talbot, C. B., Kempf, A., Omoto, J. J., Hartenstein, V., & Miesenböck, G. (2018). Recurrent circuitry for balancing sleep need and sleep. *Neuron*, *97*, 378–389. https://doi.org/10.1016/j.neuron.2017.12.016

el Jundi, B., Baird, E., Byrne, M. J., & Dacke, M. (2019). The brain behind straight-line orientation in dung beetles. *Journal of Experimental Biology*, *222*, jeb192450. https://doi.org/10.1242/jeb.192450

el Jundi, B., Pfeiffer, K., Heinze, S., & Homberg, U. (2014). Integration of polarization and chromatic cues in the insect sky compass. *Journal of Comparative Physiology A*, *200*, 575–589. https://doi.org/10.1007/s00359-014-0890-6

el Jundi, B., Warrant, E. J., Byrne, M. J., Khaldy, L., Baird, E., Smolka, J., & Dacke, M. (2015). Neural coding underlying the cue preference for celestial orientation. *Proceedings of the National Academy of Sciences of the United States of America*, *112*, 11395–11400. https://doi.org/10.1073/pnas.1501272112

el Jundi, B., Warrant, E. J., Pfeiffer, K., & Dacke, M. (2018). Neuroarchitecture of the dung beetle central complex. *Journal of Comparative Neurology*, *526*, 2612–2630. https://doi.org/10.1002/cne.24520

Evers, J. F., Schmitt, S., Sibila, M., & Duch, C. (2005). Progress in functional neuroanatomy: Precise automatic geometric reconstruction of neuronal morphology from confocal image stacks. *Journal of Neurophysiology*, *93*, 2331–2342. https://doi.org/10.1152/jn.00761.2004

Franconville, R., Beron, C., & Jayaraman, V. (2018). Building a functional connectome of the *Drosophila* central complex. *eLife*, *7*, e37017. https://doi.org/10.7554/eLife.37017

Green, J., Adachi, A., Shah, K. K., Hirokawa, J. D., Magani, P. S., & Maimon, G. (2017). A neural circuit architecture for angular integration in *Drosophila*. *Nature*, *546*, 101–106. https://doi.org/10.1038/nature22343

Green, J., Vijayan, V., Mussells Pires, P., Adachi, A., & Maimon, G. (2019). A neural heading estimate is compared with an internal goal to guide oriented navigation. *Nature Neuroscience*, *22*, 1460–1468. https://doi.org/10.1038/s41593-019-0444-x

Guo, F., Holla, M., Díaz, M. M., & Rosbash, M. (2018). A circadian output circuit controls sleep-wake arousal in *Drosophila*. *Neuron*, *100*, 624–635. https://doi.org/10.1016/j.neuron.2018.09.002

Guo, P., & Ritzmann, R. E. (2013). Neural activity in the central complex of the cockroach brain is linked to turning behaviors. *Journal of Experimental Biology*, *216*, 992–1002. https://doi.org/10.1242/jeb.080473

Hanesch, U., Fischbach, K.-F., & Heisenberg, M. (1989). Neuronal architecture of the central complex in *Drosophila melanogaster*. *Cell and Tissue Research*, *257*, 343–366. https://doi.org/10.1007/BF00261838

Heidel, E., & Pflüger, H.-J. (2006). Ion currents and spiking properties of identified subtypes of locust octopaminergic dorsal unpaired median neurons. *European Journal of Neuroscience*, *23*, 1189–1206. https://doi.org/10.1111/j.1460-9568.2006.04655.x

Heinze, S., Florman, J., Asokaraj, S., el Jundi, B., & Reppert, S. M. (2013). Anatomical basis of sun compass navigation II: The neuronal composition of the central complex of the monarch butterfly. *Journal of Comparative Neurology*, *521*, 267–298. https://doi.org/10.1002/cne.23214

Heinze, S., & Homberg, U. (2007). Maplike representation of celestial *E*-vector orientations in the brain of an insect. *Science*, *315*, 995–997. https://doi.org/10.1126/science.1135531

Heinze, S., & Homberg, U. (2008). Neuroarchitecture of the central complex of the desert locust: Intrinsic and columnar neurons. *Journal of Comparative Neurology*, *511*, 454–478. https://doi.org/10.1002/cne.21842

Heinze, S., & Homberg, U. (2009). Linking the input to the output: New sets of neurons complement the polarization network in the locust central complex. *Journal of Neuroscience*, *29*, 4911–4921. https://doi.org/10.1523/JNEUROSCI.0332-09.2009

Heinze, S., Narendra, A., & Cheung, A. (2018). Principles of insect path integration. *Current Biology*, *28*, R1043–R1058. https://doi.org/10.1016/j.cub.2018.04.058

Heinze, S., & Reppert, S. M. (2011). Sun compass integration of skylight cues in migratory monarch butterflies. *Neuron*, *69*, 345–358. https://doi.org/10.1016/j.neuron.2010.12.025

Held, M., Berz, A., Hensgen, R., Muenz, T. S., Scholl, C., Rössler, W., … Pfeiffer, K. (2016). Microglomerular synaptic complexes in the sky-compass network of the honeybee connect parallel pathways from the anterior optic tubercle to the central complex. *Frontiers in Behavioral Neuroscience*, *10*, 186. https://doi.org/10.3389/fnbeh.2016.00186

Homberg, U. (1985). Interneurones of the central complex in the bee brain (*Apis mellifera*, *L.*). *Journal of Insect Physiology*, *31*, 251–264. https://doi.org/10.1016/0022-1910(85)90127-1

Homberg, U. (1994). Flight-correlated activity changes in neurons of the lateral accessory lobes in the brain of the locust *Schistocerca gregaria*. *Journal of Comparative Physiology A*, *175*, 597–610. https://doi.org/10.1007/BF00199481

Homberg, U., Vitzthum, H., Müller, M., & Binkle, U. (1999). Immunocytochemistry of GABA in the central complex of the locust *Schistocerca gregaria*: Identification of immunoreactive neurons and colocalization

with neuropeptides. *Journal of Comparative Neurology*, *409*, 495–507. https://doi.org/10.1002/(SICI)1096-9861(19990705)409:3<495::AID-CNE12>3.0.CO;2-F

Honkanen, A., Adden, A., da Silva Freitas, J., & Heinze, S. (2019). The insect central complex and the neural basis of navigational strategies. *Journal of Experimental Biology*, *222*, jeb188854. https://doi.org/10.1242/jeb.188854

Immonen, E.-V., Dacke, M., Heinze, S., & el Jundi, B. (2017). Anatomical organization of the brain of a diurnal and a nocturnal dung beetle. *Journal of Comparative Neurology*, *525*, 1879–1908. https://doi.org/10.1002/cne.24169

Ito, K., Shinomiya, K., Ito, M., Armstrong, J. D., Boyan, G., Hartenstein, V., … Vosshall, L. B. (2014). A systematic nomenclature for the insect brain. *Neuron*, *81*, 755–765. https://doi.org/10.1016/j.neuron.2013.12.017

Jonescu, C. N. (1909). Vergleichende Untersuchungen über das Gehirn der Honigbiene. *Jenaische Zeitschrift für Naturwissenschaft*, *45*, 111–180.

Kahsai, L., Martin, J.-R., & Winther, A. M. E. (2010). Neuropeptides in the *Drosophila* central complex in modulation of locomotor behavior. *Journal of Experimental Biology*, *213*, 2256–2265. https://doi.org/10.1242/jeb.043190

Klagges, B. R., Heimbeck, G., Godenschwege, T. A., Hofbauer, A., Pflugfelder, G. O., Reifegerste, R., … Buchner, E. (1996). Invertebrate synapsins: A single gene codes for several isoforms in *Drosophila*. *Journal of Neuroscience*, *16*, 3154–3165. https://doi.org/10.1523/JNEUROSCI.16-10-03154.1996

Kreissl, S., Strasser, C., & Galizia, C. G. (2010). Allatostatin immunoreactivity in the honeybee brain. *Journal of Comparative Neurology*, *518*, 1391–1417. https://doi.org/10.1002/cne.22343

Lamaze, A., Krätschmer, P., Chen, K.-F., Lowe, S., & Jepson, J. E. C. (2018). A wake-promoting circadian output circuit in *Drosophila*. *Current Biology*, *28*, 3098–3105. https://doi.org/10.1016/j.cub.2018.07.024

Li, W., Pan, Y., Wang, Z., Gong, H., Gong, Z., & Liu, L. (2009). Morphological characterization of single fan-shaped body neurons in *Drosophila melanogaster*. *Cell and Tissue Research*, *336*, 509–519. https://doi.org/10.1007/s00441-009-0781-2

Lin, C.-Y., Chuang, C.-C., Hua, T.-E., Chen, C.-C., Dickson, B. J., Greenspan, R. J., & Chiang, A. S. (2013). A comprehensive wiring diagram of the protocerebral bridge for visual information processing in the *Drosophila* brain. *Cell Reports*, *3*, 1739–1753. https://doi.org/10.1016/j.celrep.2013.04.022

Liu, G., Seiler, H., Wen, A., Zars, T., Ito, K., Wolf, R., … Liu, L. (2006). Distinct memory traces for two visual features in the *Drosophila* brain. *Nature*, *439*, 551–556. https://doi.org/10.1038/nature04381

Milde, J. J. (1988). Visual responses of interneurones in the posterior median protocerebrum and the central complex of the honeybee *Apis mellifera*. *Journal of Insect Physiology*, *34*, 427–436. https://doi.org/10.1016/0022-1910(88)90113-8

Mobbs, P. G. (1985). Brain structure. In G. A. Kerkut & L. I. Gilbert (Eds.), *Comprehensive insect physiology, biochemistry, and pharmacology, vol. 5: Nervous system: Structure and motor function* (pp. 299–370). Oxford: Pergamon Press.

Müller, M., Homberg, U., & Kühn, A. (1997). Neuroarchitecture of the lower division of the central body in the brain of the locust (*Schistocerca gregaria*). *Cell and Tissue Research*, *288*, 159–176. https://doi.org/10.1007/s004410050803

Neuser, K., Triphan, T., Mronz, M., Poeck, B., & Strauss, R. (2008). Analysis of spatial orientation memory in *Drosophila*. *Nature*, *453*, 1244–1247. https://doi.org/10.1038/nature07003

Ofstad, T. A., Zuker, C. S., & Reiser, M. B. (2011). Visual place learning in *Drosophila melanogaster*. *Nature*, *474*, 204–207. https://doi.org/10.1038/nature10131

Omoto, J. J., Keleş, M. F., Nguyen, B.-C. M., Bolanos, C., Lovick, J. K., Frye, M. A., & Hartenstein, V. (2017). Visual input to the *Drosophila* central complex by developmentally and functionally distinct neuronal populations. *Current Biology*, *27*, 1098–1110. https://doi.org/10.1016/j.cub.2017.02.063

Omoto, J. J., Nguyen, B.-C. M., Kandimalla, P., Lovick, J. K., Donlea, J. M., & Hartenstein, V. (2018). Neuronal constituents and putative interactions within the *Drosophila* ellipsoid body neuropil. *Frontiers in Neural Circuits*, *12*, 103. https://doi.org/10.3389/fncir.2018.00103

Ott, S. R. (2008). Confocal microscopy in large insect brains: Zinc-formaldehyde fixation improves synapsin immunostaining and preservation of morphology in whole-mounts. *Journal of Neuroscience Methods*, *172*, 220–230. https://doi.org/10.1016/j.jneumeth.2008.04.031

Pegel, U. (2018). *Processing of sky compass cues and wide-field motion in the central complex of the desert locust (Schistocerca gregaria)*. (Doctoral dissertation). https://doi.org/10.17192/z2018.0252

Pegel, U., Pfeiffer, K., & Homberg, U. (2018). Integration of celestial compass cues in the central complex of the locust brain. *Journal of Experimental Biology*, *221*, jeb171207. https://doi.org/10.1242/jeb.171207

Pegel, U., Pfeiffer, K., Zittrell, F., Scholtyssek, C., & Homberg, U. (2019). Two compasses in the central complex of the locust brain. *Journal of Neuroscience*, *39*, 3070–3080. https://doi.org/10.1523/JNEUROSCI.0940-18.2019

Pfeiffer, K., & Homberg, U. (2014). Organization and functional roles of the central complex in the insect brain. *Annual Review of Entomology*, *59*, 165–184. https://doi.org/10.1146/annurev-ento-011613-162031

Phillips-Portillo, J. (2012). The central complex of the flesh fly, *Neobellieria bullata*: Recordings and morphologies of protocerebral inputs and small-field neurons. *Journal of Comparative Neurology*, *520*, 3088–3104. https://doi.org/10.1002/cne.23134

Phillips-Portillo, J., & Strausfeld, N. J. (2012). Representation of the brain's superior protocerebrum of the flesh fly, *Neobellieria bullata*, in the central body. *Journal of Comparative Neurology*, *520*, 3070–3087. https://doi.org/10.1002/cne.23094

Poeck, B., Triphan, T., Neuser, K., & Strauss, R. (2008). Locomotor control by the central complex in *Drosophila* – An analysis of the *tay bridge* mutant. *Developmental Neurobiology*, *68*, 1046–1058. https://doi.org/10.1002/dneu.20643

Rosner, R., & Homberg, U. (2013). Widespread sensitivity to looming stimuli and small moving objects in the central complex of an insect brain. *Journal of Neuroscience*, *33*, 8122–8133. https://doi.org/10.1523/JNEUROSCI.5390-12.2013

Schäfer S., Bicker G. (1986). Distribution of GABA-like immunoreactivity in the brain of the honeybee. *Journal of Comparative Neurology*, *246*, (3), 287–300. http://dx.doi.org/10.1002/cne.902460302.

Schmitt, S., Evers, J. F., Duch, C., Scholz, M., & Obermayer, K. (2004). New methods for the computer-assisted 3-D reconstruction of neurons from confocal image stacks. *NeuroImage*, *23*, 1283–1298. https://doi.org/10.1016/j.neuroimage.2004.06.047

Schürmann, F. W., & Klemm, N. (1984). Serotonin-immunoreactive neurons in the brain of the honeybee. *Journal of Comparative Neurology*, *225*, 570–580. https://doi.org/10.1002/cne.902250407

Seelig, J. D., & Jayaraman, V. (2013). Feature detection and orientation tuning in the *Drosophila* central complex. *Nature*, *503*, 262–266. https://doi.org/10.1038/nature12601

Shiozaki, H. M., & Kazama, H. (2017). Parallel encoding of recent visual experience and self-motion during navigation in *Drosophila*. *Nature Neuroscience*, *20*, 1395–1403. https://doi.org/10.1038/nn.4628

Sinakevitch, I., Niwa, M., & Strausfeld, N. J. (2005). Octopamine-like immunoreactivity in the honey bee and cockroach: Comparable organization in the brain and subesophageal ganglion. *Journal of Comparative Neurology*, *488*, 233–254. https://doi.org/10.1002/cne.20572

Stone, T., Webb, B., Adden, A., Weddig, N. B., Honkanen, A., Templin, R., … Heinze, S. (2017). An anatomically constrained model for path integration in the bee brain. *Current Biology*, *27*, 3069–3085. https://doi.org/10.1016/j.cub.2017.08.052

Strauss, R., & Heisenberg, M. (1993). A higher control center of locomotor behavior in the *Drosophila* brain. *Journal of Neuroscience*, *13*, 1852–1861. https://doi.org/10.1523/JNEUROSCI.13-05-01852.1993

Träger, U., Wagner, R., Bausenwein, B., & Homberg, U. (2008). A novel type of microglomerular synaptic complex in the polarization vision pathway of the locust brain. *Journal of Comparative Neurology*, *506*, 288–300. https://doi.org/10.1002/cne.21512

Turner-Evans, D., Wegener, S., Rouault, H., Franconville, R., Wolff, T., Seelig, J. D., … Jayaraman, V. (2017). Angular velocity integration in a fly heading circuit. *eLife*, *6*, e23496. https://doi.org/10.7554/eLife.23496

Vitzthum, H., Müller, M., & Homberg, U. (2002). Neurons of the central complex of the locust *Schistocerca gregaria* are sensitive to polarized light. *Journal of Neuroscience*, *22*, 1114–11125. https://doi.org/10.1523/JNEUROSCI.22-03-01114.2002

von Frisch, K. (1946). Die Sprache der Bienen und ihre Nutzanwendung in der Landwirtschaft. *Experientia*, *2*, 397–404. https://doi.org/10.1007/BF02154212

von Frisch K. (1949). Die Polarisation des Himmelslichtes als orientierender Faktor bei den Tänzen der Bienen. *Experientia*, *5*, (4), 142–148. http://dx.doi.org/10.1007/bf02174424.

von Hadeln, J., Althaus, V., Häger, L., & Homberg, U. (2018). Anatomical organization of the cerebrum of the desert locust *Schistocerca gregaria*. *Cell and Tissue Research*, *374*, 39–62. https://doi.org/10.1007/s00441-018-2844-8

von Hadeln, J., Hensgen, R., Bockhorst, T., Rosner, R., Heidasch, R., Pegel, U., … Homberg, U. (2020). Neuroarchitecture of the central complex of the desert locust: Tangential neurons. *Journal of Comparative Neurology*, *528*, 906–934. https://doi.org/10.1002/cne.24796

Weir, P. T., & Dickinson, M. H. (2015). Functional divisions for visual processing in the central brain of flying *Drosophila*. *Proceedings of the National Academy of Sciences of the United States of America*, *112*, E5523–E5532. https://doi.org/10.1073/pnas.1514415112

Wendt, B., & Homberg, U. (1992). Immunocytochemistry of dopamine in the brain of the locust *Schistocerca gregaria*. *Journal of Comparative Neurology*, *321*, 387–403. https://doi.org/10.1002/cne.903210307

Williams, J. L. D. (1975). Anatomical studies of the insect central nervous system: A ground-plan of the midbrain and an introduction to the central complex in the locust, *Schistocerca gregaria* (Orthoptera). *Journal of Zoology*, *176*, 67–86. https://doi.org/10.1111/j.1469-7998.1975.tb03188.x

Wolff, T., Iyer, N. A., & Rubin, G. M. (2015). Neuroarchitecture and neuroanatomy of the *Drosophila* central complex: A Gal4-based dissection of protocerebral bridge neurons and circuits. *Journal of Comparative Neurology*, *523*, 997–1037. https://doi.org/10.1002/cne.23705

Wolff, T., & Rubin, G. M. (2018). Neuroarchitecture of the *Drosophila* central complex: A catalog of nodulus and asymmetrical body neurons and a revision of the protocerebral bridge catalog. *Journal of Comparative Neurology*, *526*, 2585–2611. https://doi.org/10.1002/cne.24512

Zeller, M., Held, M., Bender, J., Berz, A., Heinloth, T., Hellfritz, T., & Pfeiffer, K. (2015). Transmedulla neurons in the sky compass network of the honeybee (*Apis mellifera*) are a possible site of circadian input. *PLoS One*, *10*, e0143244. https://doi.org/10.1371/journal.pone.0143244

How to cite this article: Hensgen R, England L, Homberg U, Pfeiffer K. Neuroarchitecture of the central complex in the brain of the honeybee: Neuronal cell types. *J Comp Neurol*. 2021;529:159–186. https://doi.org/10.1002/cne.24941